The Type II supernovae 2006V and 2006au: two SN 1987A-like events[⋆]

F. Taddia[1], M. D. Stritzinger[1,2], J. Sollerman[1], M. M. Phillips[3], J. P. Anderson[4], M. Ergon[1], G. Folatelli[5], C. Fransson[1], W. Freedman[6], M. Hamuy[4], N. Morrell[3], A. Pastorello[7,8], S. E. Persson[6], and S. Gonzalez[3]

[1] Department of Astronomy, The Oskar Klein Center, Stockholm University, AlbaNova, 10691 Stockholm, Sweden
[2] *Affiliated member* Dark Cosmology Centre, Niels Bohr Institute, University of Copenhagen, Juliane Maries Vej 30, 2100 Copenhagen Ø, Denmark
[3] Carnegie Observatories, Las Campanas Observatory, Casilla 601, La Serena, Chile
[4] Universidad de Chile, Departamento de Astronomía, Casilla 36-D, Santiago, Chile
[5] Institute for the Physics and Mathematics of the Universe (IPMU), University of Tokyo, 5-1-5 Kashiwanoha, Kashiwa, Chiba 277-8583, Japan
[6] Observatories of the Carnegie Institution for Science, 813 Santa Barbara St., Pasadena, CA 91101, USA
[7] Astrophysics Research Centre, School of Mathematics and Physics, Queen University Belfast, Belfast BT7 1NN, United Kingdom
[8] INAF - Osservatorio Astronomico di Padova, Vicolo dell'Osservatorio 5, I-35122, Padova, Italy

Abstract

Context. Supernova 1987A revealed that a blue supergiant (BSG) star can end its life as a core-collapse supernova (SN). SN 1987A and other similar objects exhibit properties that distinguish them from ordinary Type II Plateau (IIP) SNe, whose progenitors are believed to be red supergiants (RSGs). Similarities among 1987A-like events include a long rise to maximum, early luminosity fainter than that of normal Type IIP SNe, and radioactivity acting as the primary source powering the light curves.
Aims. We present and analyze two SNe monitored by the Carnegie Supernova Project that are reminiscent of SN 1987A.
Methods. Optical and near-infrared (NIR) light curves, and optical spectroscopy of SNe 2006V and 2006au are presented. These observations are compared to those of SN 1987A, and are used to estimate properties of their progenitors.
Results. Both objects exhibit a slow rise to maximum and light curve evolution similar to that of SN 1987A. At the earliest epochs, SN 2006au also displays an initial dip which we interpret as the signature of the adiabatic cooling phase that ensues shock breakout. SNe 2006V and 2006au are both found to be bluer, hotter and brighter than SN 1987A. Spectra of SNe 2006V and 2006au are similar to those of SN 1987A and other normal Type II objects, although both consistently exhibit expansion velocities higher than SN 1987A. Semi-analytic models are fit to the UVOIR light curve of each object from which physical properties of the progenitors are estimated. This yields ejecta mass estimates of $M_{ej} \approx 20\,\mathrm{M}_\odot$, explosion energies of $E \approx 2 - 3 \times 10^{51}$ erg, and progenitor radii of $R \approx 75 - 100\,\mathrm{R}_\odot$ for both SNe.
Conclusions. The progenitors of SNe 2006V and 2006au were most likely BSGs with a larger explosion energy as compared to that of SN 1987A.

Key words. supernovae: general – supernovae: individual: SN 2006V, SN 2006au, SN 1987A

1. Introduction

It is believed that hydrogen rich stars with masses larger than $\sim 8\,\mathrm{M}_\odot$ end their lives as Type II supernovae (SNe II). Such supernovae typically reach peak brightness on time scales of days to a few weeks after explosion, and often this is followed by a "plateau" phase lasting up to several months. The plateau phase is produced by the recombination of hydrogen in the ejecta and provides the namesake to the sub-type designated as Type IIP SNe (SNe IIP). Both theory and observations converge in asserting that the progenitors of SNe IIP are red supergiants (RSGs, see e.g. Grassberg et al. 1971). On the observational side, this can be inferred from the length of the plateau phase (Popov

1993), and the progenitors themselves, having in a handful of cases been identified in pre-explosion images (see Smartt 2009).

The best ever studied supernova – SN 1987A – showed that blue supergiants (BSGs) also produce SNe IIP, although with somewhat peculiar light curves. In this case the early bolometric luminosity was considerably smaller than for a typical SN IIP, suggesting that the majority of the explosion energy was used to adiabatically expand the compact BSG star. The light curves of SN 1987A displayed an unusually long rise to maximum and were mainly powered by the radioactive decay of ^{56}Ni and its daughter product ^{56}Co (see Arnett et al. 1989 for a review on SN 1987A, including a discussion on its progenitor).

Given the impact of SN 1987A on our general understanding of SN physics, identifying additional objects which have BSG progenitors is of importance. Following the discovery of SN 1987A and its association with a BSG, 11 years passed before another similar SN was found. Like its predecessor, SN 1998A displayed a ~ 100 day rise to maximum. It also exhibited higher expansion velocities and was more luminous

---

(Woodings et al. 1998; Pastorello et al. 2005) than SN 1987A. Pastorello et al. (2005) argued that the progenitor of SN 1998A was a BSG. Kleiser et al. (2011) recently published a study of two other objects, SNe 2000cb and 2005ci, that may also have a BSG origin, and most recently, Pastorello et al. (2011) presented observations of SN 2009E which they argue to have a BSG progenitor as well.

In this paper we present observations obtained within the *Carnegie Supernova Project* (CSP; Hamuy et al. 2006) of the 1987A-like SNe 2006V and 2006au. We investigate the properties of these two SNe and compare their photometric and spectroscopic characteristics to SN 1987A and other peculiar SNe II. We find that these two objects have similar light curve shapes and spectral properties as SN 1987A. In what follows our data set is used to place limits on the physical parameters of their compact progenitor stars. From this analysis we suggest the progenitors of these SNe were BSGs.

SN 2006V was discovered on 4.7 February 2006 UT (Chen et al. 2006) in the SAB(rs) galaxy UGC 6510 during the course of the Taiwan Supernova Survey. With J2000.0 coordinates $\alpha = 11^{\rm h}31^{\rm m}30.01^{\rm s}$, $\delta = -01°17'52''.2$, the SN was positioned $32''.1$ West and $40''.4$ North from the host galaxy center (see Fig. 1). On 7.5 February UT, Blondin et al. (2006) spectroscopically classified SN 2006V as a Type II SN, and noted the absorption in Hα to be blue-shifted by roughly 4000 km s^{-1}. According to the Nasa Extragalactic Database (NED), UGC 6510 has a heliocentric redshift $z = 0.0158$. From the narrow Hα emission line measured in the optical spectra presented below, we measure a value of $z = 0.0157 \pm 0.0013$ (the error corresponds to an uncertainty of ± 400 km s^{-1}). Adopting a Hubble constant of H$_0 = 73.8 \pm 2.4$ km s^{-1} Mpc^{-1} (Riess et al. 2011) our measured redshift from the spectra of SN 2006V corresponds to a distance of 72.7 ± 5.0 Mpc. Here we have taken into account peculiar motion corrections (Virgo+GA+Shapley, see Mould et al. 2000) and cosmological parameters of $\Omega_m = 0.30$ and $\Omega_\Lambda = 0.70$.

SN 2006au was discovered on 7.2 March 2006 UT in the Scd galaxy UGC 11057 by the Tenagra Observatory Supernova Search (Trondal et al. 2006). With J2000.0 coordinates $\alpha = 17^{\rm h}57^{\rm m}13.56^{\rm s}$, $\delta = 12°11'03''.2$, this object was located $17''.0$ West and $18''.2$ North from the center of the host galaxy (see Fig. 2). On 13.6 March UT, Blanc et al. (2006) classified SN 2006au as a Type II SN, and noted a well developed Hα P-Cygni profile. NED lists a heliocentric redshift to UGC 11057 of $z = 0.0099$, which is in agreement with the value measured from our spectra of $z = 0.0098 \pm 0.0013$. Our measured redshift to UGC 11057 corresponds to a distance of 46.2 ± 3.2 Mpc, where we again adopted the above-mentioned cosmology and peculiar motions.

The organization of this paper is as follows: Section 2 contains brief details regarding the observations and subsequent data reduction techniques; Section 3 presents the broad-band optical and near-infrared photometry; Section 4 contains the spectroscopic observations; Section 5 gives our discussion including a comparison with other 1987A-like objects and SNe from BSGs; and this is followed by our conclusions in Section 6.

2. Data Acquisition and Reduction

Broad-band imaging of SNe 2006V and 2006au was obtained with facilities at the Las Campanas Observatory (LCO). Optical ($ugriBV$) and near-infrared (YJH) imaging was performed with the Henrietta Swope 1-m and the Irénée du Pont 2.5-m telescopes equipped with CSP filters. The optical images were obtained with the Swope Direct Camera equipped with the CCD named Site 3, and with the du Pont Direct Camera equipped with the CCD named Tek 5. In the following we adopt Site 3 and Tek 5 as names to distinguish these cameras. Near-infrared imaging was obtained with RetroCam on Swope and with the Wide Field IR Camera (WIRC) on the du Pont. Details regarding these instruments and the bandpasses used are given in Hamuy et al. (2006), Contreras et al. (2010), and Stritzinger et al. (2011).

Detailed descriptions of the observing techniques and data reduction methodology can be found in Contreras et al. (2010); in what follows we briefly summarize the data reduction process. All optical images were reduced in a standard manner including: (i) bias subtraction, (ii) flat-field division, and (iii) the application of a shutter time and linearity correction. The near-infrared images were also reduced following several steps, consisting of (i) dark subtraction, (ii) flat-field division, (iii) sky subtraction, and (iv) geometric alignment and combination of the dithered frames.

Months after each SN faded, deep template images of their host galaxy were obtained under excellent seeing conditions. Optical and near-infrared template imaging was performed with the du Pont telescope using Tek 5 and WIRC. Following the method highlighted in Contreras et al. (2010), the template images allow us to subtract away the host background light at the position of the SN in each science image.

Observed magnitudes of each SN were computed differentially from the science frames with respect to a local sequence of stars. The photometric sequences were calibrated using Landolt (1992) (BV), Smith et al. (2002) ($ugri$) and Persson et al. (1998) (YJH) fields observed over a minimum of three photometric nights. The local sequences of SNe 2006V and 2006au in the standard system are provided in Table 1.

Nine epochs of optical spectroscopy were obtained for both SNe 2006V and 2006au with telescopes at LCO, and in one instance each, with the New Technology Telescope (NTT). A journal of the spectroscopic observations is provided in Table 2. Depending on the exact instrument used, the wavelength interval generally ranges from ~ 3800 Å to 9500 Å. Standard reductions of each spectrum were performed as described in Hamuy et al. (2006). Briefly, this consisted of overscan correction, bias subtraction and flat-fielding. The 2-D spectra were then optimally extracted and wavelength calibrated with respect to arc lamps. The wavelength corrected spectra were corrected for telluric absorption through the division of a telluric standard spectrum, and then flux-calibrated. Multiple exposures of a particular object were then combined to produce a final high signal-to-noise science product. This allowed for the removal of cosmic rays.

3. Photometry

Optical and near-infrared light curves of SNe 2006V and 2006au are plotted in Figs. 3 and 4, respectively. The corresponding optical photometry – in the CSP natural system – is listed in Tables 3 and 5, whereas the final near-IR photometry in the Persson et al. (1998) system is listed in Tables 4 and 6. The differences in measured magnitudes between the natural and the standard system are insignificant for the purpose of this study (Hamuy et al. 2006), whereas they would be important for precision cosmology. The transformation equations between the two systems are reported in Hamuy et al. (2006), with updated color terms provided by Stritzinger et al. (2011). The light curves of SN 2006V follow the flux evolution from -50 to $+75$ days past B-band maximum ($B_{\rm max}$, i.e. $JD = 2453823.7$), while

those of SN 2006au range from -59 to $+33$ days past $B_{\max}$ ($JD = 2453865.5$).

The long rise to maximum, the broad peak and the subsequent decline to the radioactive tail are very similar to those shown by the light curve of SN 1987A. This is evident in Figs. 3 and 4, where we have also included for comparison the light curves of SN 1987A as thin solid lines. In particular, we show U- and I-band from Hamuy et al. (1988) and J- and H-band from Bouchet et al. (1989). B, g, V and r light curves of SN 1987A are synthetic magnitudes, which have been computed using CSP bandpasses and spectrophotometry published by Phillips et al. (1988).

Although both SNe 2006V and 2006au were spectroscopically classified as SNe II (Blanc et al. 2006; Blondin et al. 2006) their sustained rise to, and evolution through maximum, suggests they are more appropriately termed peculiar 1987A-like SNe (see also Pastorello et al. 2011).

Taking a closer look at the early phase evolution of SN 2006au, reveals that the light curves first decrease in brightness on a time-scale of $\sim 2 - 3$ weeks. This is most evident in the B, i and r bands (the unfiltered/r magnitudes from discovery and confirmation images, Trondal et al. 2006, confirm this trend), followed to a lesser extent in the gV bands while the evolution in YJH is nearly flat.

A similar evolution was observed in the U- and B-band light curves of SN 1987A (Hamuy et al. 1988), as well as in other core-collapse SNe caught just after explosion; e.g. SNe 1993J (Richmond et al. 1994), 1999ex (Stritzinger et al. 2002), 2008D (Malesani et al. 2009; Modjaz et al. 2009) and 2011dh (Soderberg et al. 2011). For these objects, that were all caught very early, this light curve evolution was interpreted as a sign of the photospheric cooling phase that ensues shock-wave breakout. The decreasing phase is not as evident in SN 2006au, but we propose a similar scenario for this supernova although its somewhat later discovery (see subsection 5.1) does not allow to see a clearly decreasing temperature at early epochs (see middle panel in Fig. 14).

The last photometric observations of SNe 2006V and 2006au were obtained at $+75$ and $+33$ days past $B_{\max}$, respectively. For this reason, we can only observe the linear decay phase for SN 2006V, whose optical light curves settle onto a similar radioactive decay slope as did SN 1987A. For SN 2006au no later phase data are available to map out the linear decline phase. However, we do note that at epochs later than $+30$ days past $B_{\max}$, the evolution appears to be faster than in the case of SN 1987A.

In order to estimate the absolute magnitudes and luminosities of SNe 2006V and 2006au, accurate estimates of Galactic reddening and reddening associated with dust in the host galaxies are needed. In the case of SN 2006V, NED lists a Galactic color excess value of $E(B - V)_{\mathrm{MW}} = 0.029$ mag (Schlegel et al. 1998). Close examination of our spectroscopic sequence of this object (Sect. 4) shows no evidence for Na I D absorption. The presence of Na I D is often considered to be a proxy for dust attenuation, therefore the lack of Na I D combined with the position of SN 2006V in the outskirts of its face-on galaxy suggests minimal host extinction. In the following we therefore assume zero host extinction for SN 2006V. Adopting the standard total-to-selective extinction value of $R_V = 3.1$ (Cardelli et al. 1989) the total color excess in the direction of SN 2006V corresponds to a modest $A_V = 0.09$ mag.

The Galactic color excess in the direction of SN 2006au is $E(B-V)_{\mathrm{MW}} = 0.172$ mag (Schlegel et al. 1998). Conspicuous Na I D absorption lines at the redshift of UGC 11057 are de-

tected in the first spectrum of SN 2006au. This is shown in the inset of Fig. 8. Two Gaussian profiles were fit to the (unresolved) Na I D lines and a total equivalent width of 0.88 ± 0.11 Å is measured. Using the Turatto et al. (2003) correlation between the Na I D equivalent width and host galaxy reddening suggests a host galaxy color excesses $E(B - V)_{host} = 0.141$ mag. This value might be affected by large uncertainty and lead to an overestimated host extinction, since we know that the Turatto et al. (2003) relation presents large scatter (see Poznanski et al. 2011). However, we combined this value with the Galactic color excess, obtaining $E(B - V)_{tot} = 0.312$ mag, which corresponds to $A_V = 0.97$ mag.

Armed with estimates of $E(B - V)_{tot}$, the absolute magnitudes of SNe 2006V and 2006au are computed for each observed bandpass. Their peak values are given in Table 7. Compared to SN 1987A, SNe 2006V and 2006au are brighter in all bands. To demonstrate the differences, in Fig. 5 the absolute B-, V- and J-band light curves of SNe 2006au and 2006V are compared to those of SN 1987A. SNe 2006V and 2006au show an absolute B magnitude difference to SN 1987A of ~ 1.5 mag and ~ 1.3 mag respectively. The differences in the V band are smaller (~ 1.0 and ~ 0.7 mag) and in the J band are further reduced (~ 0.8 and ~ 0.5 mag).

To gain insight into the photospheric temperatures, we plot in Fig. 6 the $B-V$, $V-r$ and $J-H$ color curves of SNe 2006V and 2006au. The plot also includes the colors of SN 1987A. The photometry of each SN has been corrected for extinction adopting the values previously mentioned. Overall the optical colors of SNe 2006V and 2006au are bluer than for SN 1987A, particularly during the earliest epochs where the $B - V$ (top panel) and $V - r$ (middle panel) color differences amount to ~ 0.7 mag and ~ 0.3 mag, respectively. Later, around $B_{\max}$, the $B - V$ colors of our two objects evolve towards the red, and are at day $+35$ comparable to the $B - V$ color of SN 1987A. The $V - r$ color of SN 2006au follows a similar evolution (at the earliest epoch it is bluer than SN 1987A by ~ 0.3 mag). In contrast, the $V - r$ color of SN 2006V is bluer than SN 1987A at all epochs. The near-infrared color $J - H$ (bottom panel) of SN 2006V is found to be similar to SN 1987A at all epochs, whereas for SN 2006au it is slightly bluer at the earliest phase (by ~ 0.1 mag).

The color comparisons suggest that the photospheres of SNe 2006V and 2006au are at higher temperatures than for SN 1987A. This is confirmed by black-body fits to the spectral energy distributions (SEDs) obtained from each photometric epoch; see middle panel in Fig. 14. As shown in this plot, the black-body temperatures of SNe 2006V and 2006au are higher than for SN 1987A. We excluded u and B from the fits, given their significant deviation from the Planck function.

4. Spectroscopy

Spectroscopic sequences of SNe 2006V and 2006au are plotted in Figs. 7 and 8, respectively. The spectra of SN 2006V cover the flux evolution from day -44 to $+25$ relative to $B_{\max}$, and for SN 2006au from day -56 to -14. The spectra of both objects exhibit common features typically observed in SNe II.

The earliest spectra of SN 2006V show all the typical features of a normal SN IIP at one month after the explosion. Together with spectral lines that are expected to be visible already at early phases (Hα, Hβ, Ca H&K and the NIR triplet), the Na I doublet and Fe II lines become prominent, particularly those of the Fe II multiplet 42.

Later on, weak lines of Sc II (5527 Å, 5641-5669 Å, 6246 Å) and the unblended Ba II λ6162 are clearly visible. The subse-

quent spectra of SN 2006V show a modest evolution with the continuum becoming marginally redder with time. Strong line blanketing can be observed below ∼4400 Å. This is probably due to the increasing strength of lines of Cr II, Ti II, Fe I. In post-maximum spectra of SN 2006V a hint of the nebular Ca II 7291-7323 Å is seen.

The spectra of SN 2006au are contaminated by the host galaxy background. A number of narrow lines due to underlying H II regions are identified including: Hα, Hβ, [O III]. Nevertheless, the spectra of SN 2006au show an evident evolution, with Na I, Sc II and Ba II lines becoming more prominent with time. This is in good agreement with the fact that the first spectrum for SN 2006au was taken at an earlier phase than for SN 2006V. Unfortunately post-maximum spectra showing nebular features are not available for SN 2006au.

Plotted in Fig. 9 are the Hα profiles as a function of time. In the case of SN 2006au the minimum of the absorption clearly evolves towards lower velocities, while in SN 2006V, where the spectra were obtained at later epochs, the Hα velocity is nearly constant at ∼ 6000 km s^{-1}. This is quantitatively shown in Fig. 10 where the expansion velocities of Hα (top panel), Hβ (middle panel) and the Fe II multiplet 42 (bottom panel) are measured from the minimum of their respective absorption features. Also included in this figure are the expansion velocities of SN 1987A measured from spectra published by Phillips et al. (1988). Following Meaburn et al. (1995), the spectra of SN 1987A were corrected for a redshift of $\Delta v = 286$ km s^{-1}. The expansion velocities of SN 2006au are clearly higher than for both of the other two objects, while SN 2006V shows marginally higher velocities than SN 1987A at nearly all epochs when we look at the Fe II lines, which are indicative of the photospheric velocity.

Finally, in Fig. 11 we compare spectra taken 2 weeks before maximum of SNe 1987A, 2006V and 2006au. Each spectrum has been corrected for extinction and redshift. In line with the color evolution, the spectra of SNe 2006V and 2006au appear to be bluer than those of SN 1987A. The blue region of the spectra is heavily suppressed in SN 1987A, whereas for SN 2006V and SN 2006au the flux is not much lower than in the red region. Indeed, for our objects, the shape of the spectral continuum is well approximated by a black body function of relatively high (∼6000 K) and almost constant temperature. Many of the common spectral features observed in typical SNe IIP are observed in the spectra of all three SNe, although the strength of several of the lines in the red portion of SN 1987A's spectrum appear to be larger. This is particularly the case for Na I and Ba II $\lambda6142$. The strong Ba II absorption line was suggested to be a signature of s-process element enhancements in the progenitor of SN 1987A (Williams 1987, but see also Utrobin & Chugai 2005).

Our objects exhibit fainter Ba II features than SN 1987A (as is also the case for SN 2009E, see Pastorello et al. 2011). That is likely due to the higher temperature of the photosphere (see Fig. 14, middle panel). This can be verified noting that objects showing stronger Ba II lines have also lower temperatures (SN 1997D, Turatto et al. 1998, and similar events, and the previously mentioned SNe 2009E and 1987A), whereas high ejecta temperature objects only show hints of such lines (or nothing at all; see e.g. SN 2009kf, Botticella et al. 2010). However, intrinsic differences in the composition can not be excluded. Williams (1987) also considered Sr II lines as a signature of s-process element enhancements. Both our objects exhibit a strong absorption line at 4077 Å which might be associated with this ion. In addition, the overall line locations in SN 2006au are shifted to the

blue compared to the other objects, which is expected from what was shown in Fig. 10.

5. Analysis and discussion

The remarkable similarity between the light curve shapes of SNe 2006V and 2006au compared to SN 1987A suggests that these objects are also mainly powered by the radioactive decay of ^{56}Ni. Moreover, early luminosities of SN 1987A-like events are fainter than those of normal SNe IIP (see e.g. Bersten & Hamuy 2009). This is consistent with a scenario involving a relatively compact progenitor star which spends the majority of its explosion energy on adiabatic expansion.

In order to derive the physical parameters of the progenitors, a reasonably accurate estimation of the explosion dates and the computation of the bolometric light curves are required. In the following two subsections we discuss the methods and the results concerning these two aspects.

5.1. Explosion dates from the expanding photospheric method

Using the light curve of SN 1987A as a template, Pastorello et al. (2005) assumed that the peak for SN 1998A was coincident in phase with the peak of SN 1987A. This was also consistent with the constraints from the last non-detection epoch close to discovery.

The discovery date of SN 2006V is $t_{disc}(06V) = 2453771.2 \ JD$, about 45 days from the last non-detection, $t_{nd}(06V) = 2453726.4 \ JD$ (Chen et al. 2006). For SN 2006au this interval is even longer, since the discovery, $t_{disc}(06au) = 2453801.7 \ JD$, occured more than one year since the previous non-detection, $t_{nd}(06au) = 2453265.65 \ JD$ (Trondal et al. 2006).

Therefore we explore an alternative approach for the determination of the explosion date. Having a set of 9 spectra for each SN, we used the expanding photospheric method (EPM), as presented by Jones et al. (2009). This method is generally used to find the distance of SNe IIP. In our case we have already an independent measure of the distance (D) and we can instead use the EPM to constrain the explosion date (t_0), by using the following procedure:

(i) We checked and, if necessary, adjusted the flux-calibration of our observed spectra by matching synthetic photometry to the broad-band photometry.

(ii) We then computed synthetic magnitudes in the Johnson-Kron-Cousin VI filters from each redshift-corrected spectrum. Here only spectra obtained prior to B_{max} were considered since the EPM method is most reliable at these phases.

(iii) A black-body spectrum was fit to the VI synthetic magnitudes in order to estimate the temperature, T, and thereby the photospheric radius divided by the SN distance, R/D, multiplied by the dilution factor, ζ. In the SN ejecta the thermalization surface emits radiation, which is diluted by scattering before reaching the observer. The dilution is mainly affected by the temperature, as shown in Eastman et al. (1996) and Dessart & Hillier (2005).

(iv) The dilution factor is estimated according to Jones et al. (2009, see their Table 2) using the expression given for temperatures computed from V and I-band synthetic magnitudes and redshift $z = 0$. In doing so the expression based on the atmosphere modeling of Dessart & Hillier (2005) was adopted. The small dependence of the dilution factor on density is ignored.

(v) For each spectrum we considered the velocity, v, obtained from the blueshift of the Fe II $\lambda5169$ absorption, which is a reasonable proxy for the photosphere velocity (e.g. Dessart & Hillier 2005, see their Fig. 14).

(vi) Using $R\zeta/D = v/D(t-t_0)$, an explosion date was then computed for each spectrum and the final value t_0 was obtained through their weighted mean.

The resulting explosion epochs are $t_0(06V) = 2453748 \pm 4$ JD and $t_0(06au) = 2453794 \pm 9$ JD. These explosion dates are consistent with the constraints provided by the discovery dates and by the last non-detection dates. With the aid of SNID, the first spectrum of SN 2006au, taken on JD 2453808.9, was compared to the library of spectra of SN 1987A. This exercise suggests this spectrum was most similar to SN 1987A approximately 10.9 days after the explosion. If we assume the same phase for our spectrum, a slightly later (4 days) explosion date for SN 2006au is obtained. This is consistent with the confidence interval obtained from the EPM analysis. Adopting the EPM estimate of t_0, the shock break-out cooling tail is found to cover a period of $\sim 10 - 15$ days, which is similar to that of SN 1993J (Richmond et al. 1994). In the case of SN 2006V, a SNID analysis did not provide a clear-cut estimate for the phase of our earliest spectra.

5.2. Bolometric light curves

The broad wavelength coverage afforded by our multi-band observations allows us to construct nearly complete bolometric light curves of SNe 2006V and 2006au. To do so the near-infrared light curves were first interpolated to obtained magnitudes at the epochs observed in the optical. The optical and near-infrared magnitudes were converted to flux at the effective wavelength of each filter. To overcome the lack of u-band photometry, magnitudes were extrapolated assuming, $u = B- <B-u>$, with the average $<B-u>$ measured during the rising phase. In doing so, we assumed a ±0.6 mag error in each extrapolated point. Next a cubic spline was fit to the SEDs at each observed epoch, and this is integrated over wavelength. In addition, a Rayleigh-Jeans (RJ) tail was included to the overall SED to account for flux redwards of the H band, along with a Wien tail to cover the UV flux. The resulting SEDs are plotted in Figs. 12 and 13, along with the spline fits and the UV and IR tails. We elected to fit a spline rather than a blackbody to avoid over-estimating the flux in the u and B bands (Terndrup et al. 1988). As shown by Hamuy et al. (1988), the inclusion of a Rayleigh-Jeans tail is a good approximation for the case of SN 1987A.

Plotted in Fig. 14 (top panel) are the bolometric light curves of SNe 2006V, 2006au and 1987A. Our bolometric light curve of SN 1987A differs slightly from the one in Hamuy et al. (1988) because we used a higher extinction estimate, $E(B-V)_{tot} = 0.175$ mag (Woosley et al. 1987). As indicated by these light curves, SNe 2006V and 2006au are more luminous than SN 1987A, reaching peak luminosities of $\log_{10}(L) \sim 42.25$ erg s^{-1} and $\log_{10}(L) \sim 42.2$ erg s^{-1}, respectively. The peak luminosity of SN 1987A is $\sim 50\%$ fainter, with $\log_{10}(L) \sim 41.90$ erg s^{-1}.

5.3. Physical parameters of the progenitors

With the estimates of t_0 from the EPM analysis and the computed bolometric light curves in hand, we next proceed to determine the physical parameters of the progenitors of both our SNe. Initial rough estimates of the ejected mass (M_{ej}) and of the explosion energy (E) can be obtained if we simply scale these parameters with respect to what has been determined for SN 1987A; $E_{87A} = 1.1 \times 10^{51}$ erg and $M_{ej}(87A)_{env} = 14\,M_\odot$ (Blinnikov et al. 2000). In order to do that, we can use the relation $t_d \propto (\kappa M_{ej}/v)^{1/2}$ from Arnett (1979), where t_d is the diffusion time, κ is the mean opacity, and v is a measure of the expansion velocity. The relation between the diffusion time of our objects and SN 1987A is $t_d(06V) = 0.90\,t_d(87A)$ and $t_d(06au) = 0.85\,t_d(87A)$, as measured from the time of the bolometric peaks, see top panel in Fig. 14. If we now assume the same mean opacity for each SN, and use an average ratio between the expansion velocities as measured from the Fe II at $\lambda5169$, (~ 1.4 for SN 2006V and ~ 1.7 for SN 2006au see bottom panel in Fig. 14), the ejecta mass for both objects is found to be $M_{ej} \sim 20\,M_\odot$ with corresponding ($E \propto M_{ej}v^2$) kinetic energies of a few foe. These simple estimates give a first hint on the nature of the progenitors.

From the bolometric light curve one can also constrain the amount of ^{56}Ni synthesized in the explosion. The daughter decay product of ^{56}Ni is ^{56}Co, and it is the decay of ^{56}Co to ^{56}Fe that powers the late-time light curve. Unfortunately our photometric coverage of SN 2006au does not extend beyond ~ 105 days after the explosion, so only an upper limit on the ^{56}Ni mass can be estimated. This is done by assuming the last photometric epoch belongs to the linear decay phase, where $L \propto M_{^{56}Ni}e^{-t/\tau}$. We thus obtain $M_{^{56}Ni}(06au) \leq 0.073\,M_\odot$. In contrast, the photometric coverage of SN 2006V (up to 150 days after the explosion) is sufficient to directly measure the ^{56}Ni mass from the linear decay phase. In doing so, we compute $M_{^{56}Ni}(06V) = 0.127 \pm 0.010\,M_\odot$.

Following the plateau luminosity relation presented by Popov (1993), $L \propto E^{5/6}M_{ej}^{-1/2}R^{2/3}$, and scaling with the radius of SN 1987A, $R(87A) = 3 \times 10^{12}$ cm $= 43\,R_\odot$ (Woosley 1988), a rough estimate of the progenitor radius of SNe 2006V and 2006au can be inferred. We note that this approach has been followed by Kleiser et al. (2011) for estimating the progenitor radius of SN 2000cb, although Popov (1993) developed the plateau luminosity relation for SNe whose emission was nonradioactive. Such a simple scaling implies radii of $\lesssim 50\,R_\odot$ for both objects, which clearly suggests a very compact progenitor for our objects.

To confirm these estimates of the progenitor and explosion parameters, we turn to the semi-analytic model of Imshennik & Popov (1992). This model includes cooling and recombination, and has been shown to provide a good fit to the bolometric light curve of SN 1987A (Imshennik & Popov 1992). As this model is not applicable to the earliest phases, it is fit only to the bolometric light curves of SNe 1987A, 2006V and 2006au at epochs after 40 days past explosion. Adopting a mean opacity $\kappa = 0.34$ cm^{2}g^{-1}, and the same exponential distribution of ^{56}Ni as used by Imshennik & Popov (1992) to fit the bolometric light curve of SN 1987A, M_{ej}, E, $M_{^{56}Ni}$ and R are estimated for all three objects.

In the case of SN 2006au we assume a $M_{^{56}Ni}$ that is equal to the upper limit estimated from the last photometric epoch. On the other hand, for this SN we can provide additional constraints, in particular on the progenitor radius, by using the initial dip in the light curve. This was done for SN 1987A, whose light curves also contain a shock break-out cooling tail. Chevalier (1992) provides an analytical expression for the luminosity of the early-time light curve of SN 1987A and similar SNe, in terms of E, M_{ej} and R. The luminosity function given by Chevalier (1992) is $L = 3.08 \times 10^{43}E_{51}^{0.91}M_{16M_\odot}^{-0.40}(F1/1.35)^{-0.17}R_{30R_\odot}t^{-0.34}$

5

erg s^{-1}. $F1$ is the factor by which each gas element increases in velocity from $t = 0$ to very late times. Following Chevalier (1992) we adopt $F1 = 1.35$. As this expression overestimates the luminosity of SN 1987A by a factor of 2, we scale it by this factor in order to fit the early epochs for both SNe 1987A and 2006au.

The best simultaneous fits to the bolometric light curves with the Imshennik & Popov (1992) model and the Chevalier (1992) analytic expression are shown in Fig. 14 (top panel) as dashed lines. The Imshennik & Popov (1992) model allows us to also constrain the ionization temperature, T_{ion}, which strongly affects the light curve shape, by fitting the effective temperature before B_{max} (dashed lines in the middle panel of Fig. 14). During the recombination phase the photospheric velocity estimated from Fe II $\lambda5169$ has also been fit in order to better constrain the energy and mass (dashed lines in the bottom panel of Fig. 14).

Our estimates for SN 2006V are as follows: $M_{ej}(06V) = 17.0\,\mathrm{M_\odot}$, $E(06V) = 2.4 \times 10^{51}$ erg, $M_{^{56}\mathrm{Ni}}(06V) = 0.127\,\mathrm{M_\odot}$ and $R(06V) = 75\,\mathrm{R_\odot}$.

The model for SN 2006au gives: $M_{ej}(06au) = 19.3\,\mathrm{M_\odot}$, $E(06au) = 3.2 \times 10^{51}$ erg, $M_{^{56}\mathrm{Ni}}(06au) = 0.073\,\mathrm{M_\odot}$ and $R(06au) = 90\,\mathrm{R_\odot}$.

The parameters for SN 1987A are: $M_{ej}(87A) = 11.8\,\mathrm{M_\odot}$, $E(87A) = 1.1 \times 10^{51}$ erg, $M_{^{56}\mathrm{Ni}}(87A) = 0.078\,\mathrm{M_\odot}$ and $R(87A) = 33\,\mathrm{R_\odot}$. The latter is in reasonable agreement with the values inferred from hydrodynamical simulations (Blinnikov et al. 2000).

Clearly the adopted semi-analytic model relies on significant simplifications and therefore one can not expect an exact fit to the data. However, it does provide a set of reasonable physical parameters. The mass and energy estimates of our objects are somewhat lower than those obtained from the simple scaling relations, and at the same time, are larger than those obtained for SN 1987A. The progenitor radii estimates from the semi-analytic models are larger than those estimated from the simple scalings, and somewhat larger than what is computed for the progenitor of SN 1987A. Nevertheless, our estimates on the radii suggests that the progenitors of SNe 2006V and 2006au were compact stars. Note that if the same elapsed time between epochs of explosion and maximum for SNe 2006V and 2006au had been assumed as for SN 1987A, larger estimates of mass and energy would have been obtained, especially for SN 2006au ($\sim 30\,\mathrm{M_\odot}$). The $M_{^{56}\mathrm{Ni}}$ estimate would also have been slightly enhanced, while the radius estimate would not change significantly. Even in this case the compact star scenario would be favoured.

5.4. 1987A-like and BSG Supernovae

SNe 2006V and 2006au are important additions to the small family of 1987A-like supernovae. The observational properties of these SNe are summarized by Pastorello et al. (2011), and we note that our SNe are among the best sampled in that collection. Among the five best studied 1987A-like objects (SNe 1998A, 2000cb, 2006V, 2006au and 2009E), our two SNe display the intrinsically brightest light curves (see Pastorello et al. 2011, their Table 5). Table 8 contains a summary of the derived physical parameters of these five objects. Here one can see that this family of SNe all appear to have ejecta masses of about 20 $\mathrm{M_\odot}$. The amount of ejected radioactive nickel is also consistently $\sim 0.1\,\mathrm{M_\odot}$. With the exception of SN 2009E, the members of this group are energetic versions of SN 1987A, as elaborated in

the case of SN 2000cb by Utrobin & Chugai (2011). Finally, the radii of these stars are consistently found to be relatively small ($\lesssim 100\,\mathrm{R_\odot}$). This provides the strongest argument for their progenitors to be BSGs.

We note that an estimate of the radius does not univocally determine the color of the progenitor star. Indeed some yellow and red supergiants may also have radii of $\approx 100\,\mathrm{R_\odot}$. A luminosity estimate of the progenitor is also required to infer its temperature, and this can be provided by the final epoch of the evolutionary track within the Hertzsprung-Russel (HR) diagram as computed with the STARS code (Eldridge & Tout 2004). The path is computed according to the mass estimate of each progenitor, roughly given by the ejecta mass from our model, and adding 2 $\mathrm{M_\odot}$ to account for the central compact object. The computed Zero Age Main Sequence (ZAMS) masses belong to the range 19-24 $\mathrm{M_\odot}$. The HR path for each 1987A-like SN in Table 8 is shown in Fig. 15. This shows that the progenitors of these SN 1987A-like events clearly belong to the B (blue-white) spectral type, as was also the case for the directly detected progenitor of SN 1987A (Woosley 1988). This spectral type is characterized by temperatures between 10000 and 30000 K, and we do find all the progenitors within this range. Note, however, that the evolutionary tracks from the STARS code do not actually contain $\sim 20\,\mathrm{M_\odot}$ stars which end their lives as BSGs, since in their final state they are all positioned in the RSG part of the diagram (in Fig. 15 the inversions of the evolutionary paths towards the BSG state have been drawn to be consistent with the computed radii). The physical reason why $\sim 20\,\mathrm{M_\odot}$ stars do explode as BSG was discussed already for SN 1987A (Arnett et al. 1989; Podsiadlowski 1992), but it is still not settled if this is due to metallicity or binary evolution.

In any case, the characteristic small progenitor radii in conjunction with the relatively high ejecta masses of these 1987A-like SNe allow us to reject a red supergiant origin. Even the yellow supergiant progenitors that have recently been suggested (see Maund et al. 2011, their Figure 4) favour a position in the HR diagram compatible with larger radii ($\sim 300\,\mathrm{R_\odot}$).

The final explosion of a BSG can apparently proceed in different ways, as can be seen from the diversity that is present in Table 8. It would be of interest to enlarge this sample, and to model them all in a consistent way. Such an effort is underway (see Pastorello et al. 2011). It is also clear that these events are intrinsically quite rare, and this is likely the reason why these massive BSG progenitors have not yet shown up in direct detections (Smartt 2009).

6. Conclusions

We have presented extensive observations of two SNe that have been shown to exhibit similarities to SN 1987A. Just as SN 1987A, both objects show a slow rise to the peak, with SN 2006V reaching B_{max} 76 days past explosion and SN 2006au after 72 days. Detailed inspection show, however, that these SNe display faster velocities and higher luminosities compared to SN 1987A. These observational parameters also suggest that our objects have higher explosion energies than SN 1987A.

SN 2006V shows the highest luminosity, and produced the largest amount of ^{56}Ni, $M_{^{56}\mathrm{Ni}}(06V) = 0.127\,\mathrm{M_\odot}$. For SN 2006au only an upper limit on the ^{56}Ni mass can be made, $M_{^{56}\mathrm{Ni}}(06au) \leqslant 0.073\,\mathrm{M_\odot}$. However, this is comparable to what SN 1987A produced.

A semi-analytic model was applied to the bolometric light curves of both SNe 2006V and 2006au that suggests the radii of

these objects are consistent with a BSG progenitor. When comparing the small family of objects in the literature thought to have a BSG origin, we find that their progenitors exhibit a wide range in masses, radii, explosion energies, and ^{56}Ni production.

References

Arnett, W. D. 1979, ApJ, 230, L37
Arnett, W. D., Bahcall, J. N, Kirshner, R. P, & Woosley, S. E. 1989, ARA&A, 27, 629
Bersten, M. C., & Hamuy, M. 2009, ApJ, 701, 200
Blanc, N., Copin, Y., Gangler, E., et al. 2006, CBET, 427, 1
Blinnikov, S., Lundqvist, P., Bartunov, O., Nomoto, K., & Iwamoto, K. 2000, ApJ, 532, 1132
Blondin, S., Modjaz, M., Kirshner, R., Challis, P., & Calkins, M. 2006, CBET, 392, 1
Botticella, M. T., Trundle, C., Pastorello, A., et al. 2010, ApJ, 717, L52
Bouchet P., Slezak, E., Le Bertre, T., Moneti, A., & Manfroid, J. 1989, A&AS, 80, 379
Cardelli, J. A., Clayton, G. C., & Mathis, J. S. 1989, ApJ, 345, 245
Chen, Y. T., Yang, M., Lin, C. S. 2006, CBET, 390, 1
Chevalier, R. A. 1992, ApJ, 394, 599
Contreras C., Hamuy, M., Phillips, M. M., et al. 2010, AJ, 139, 519
Dessart, L., & Hillier, D. J. 2005, A&A, 439, 671
Eastman, R. G., Schmidt, B. P., & Kirshner, R. 1996, ApJ, 466, 911
Eldridge, J. J., & Tout, C. A. 2004, MNRAS, 353, 87
Glatt, K., Grebel, E. K., & Koch, A. 2010, A&A, 517, A50
Grassberg, E. K., Imshennik, V. S., & Nadyozhin, D. K. 1971, Ap&SS, 10, 28
Hamuy, M., Folatelli, G., Morrell, N., & Phillips, M. M. 2006, PASP, 118, 2
Hamuy, M., Suntzeff, N. B., Gonzalez, R., & Martin, G. 1988, AJ, 95, 63
Imshennik, V. S., & Popov, D. V. 1992, Astron. Zh. 69, 497
Jones, M. I., Hamuy, M., Lira, P., et al. 2009, ApJ, 696, 1176
Kleiser, I. K. W., Poznanski, D., Kasen, D., et al. 2011, MNRAS, 415, 372
Landolt, A. U. 1992, AJ, 104, 340
Malesani, D., Fynbo, J. P. U., Hjorth, J., et al. 2009, ApJ, 692, L84
Maund, J. R., Fraser, M., Ergon, M., et al. 2011, arXiv:1106.2565
Meaburn, J., Bryce, M., & Holloway, A. J. 1995, A&A, 299, L1
Modjaz, M., Li, W., Butler, N., et al. 2009, ApJ, 702, 226
Mould, J. R., Huchra, J. P., Freedman, W. L., et al. 2000, ApJ, 529, 786
Pastorello, A., Baron, E., Branch, D., et al. 2005, MNRAS, 360, 950
Pastorello, A., Pumo, M. L., Havasardyan, H., et al. 2011, A&A, accepted, arXiv:submit/0355717
Persson, S. E., Murphy, D. C., Krzeminski, W., Roth, M., & Rieke, M. J. 1998, AJ, 116, 2475
Phillips, M. M., Heathcote, S. R., Hamuy, M., & Navarrete, M. 1988, AJ, 95, 1087
Podsiadlowski, P. 1992, PASP, 104, 717
Popov, D. V. 1993, ApJ, 414, 712
Poznanski, D., Ganeshalingam, M., Silverman, J. M., & Filippenko, A. V. 2011, MNRAS, 415, L81
Richmond, M. W., Treffers, R. R., Filippenko, A. V., et al. 1994, AJ, 107, 1022
Riess, A. G., Macri, L., Casertano, S., et al. 2011 ApJ, 732, 129
Schlegel, D. J., Finkbeiner, D. P., & Davis, M. 1998, ApJ, 500, 525
Smartt, S. J. 2009, ARA&A, 47, 63
Smith J. A., Tucker, D. L., Kent, S., et al. 2002, AJ, 123, 2121
Soderberg, A. M., Margutti, R., Zauderer, B. A., et al. 2011, arXiv:1107.1876
Stewart, H. A., Guinan, E. F., Wasatonic, R., Engle, S. G., & McCook, G. P. 2009, Bulletin of the American Astronomical Society, 41, #408.13
Storm, J., Carney, B. W., Gieren, W. P., et al. 2004, A&A, 415, 531
Stritzinger, M., Hamuy, M., Suntzeff, N. B., et al. 2002, AJ, 124, 2100
Stritzinger, M., Phillips, M. M., Boldt, L., et al. 2011, AJ, accepted
Terndrup, D. M., Elias, J. H., Gregory, B., et al. 1988, Proceedings of the Astronomical Society of Australia, 7, 412
Trondal, O., Luckas, P., & Schwartz, M. 2006, CBET, 426, 1

Turatto, M., Benetti, S., & Cappellaro, E. 2003, From Twilight to Highlight: The Physics of Supernovae, ed. W. Hillebrandt & B. Leibundgut (Berlin: Springer), 200
Turatto, M., Mazzali, P. A., Young, T. R., et al. 1998, ApJ, 498, L129
Utrobin, V. P., & Chugai, N. N. 2005, A&A, 441, 271
Utrobin, V. P., & Chugai, N. N. 2011, A&A, 532, A100
Williams, R. E., 1987, ApJ, 320, 117
Woodings, S., Williams, A., Martin, R., Blair, D., & Burman, R. 1998, IAU Circ., 6849, 3
Woosley, S. E. 1988, ApJ, 330, 218
Woosley, S. E., Pinto, P. A., Martin, P. G., & Weaver, T. A., 1987, ApJ, 617, 1233

Table 1.   Optical and near-infrared photometry of the local sequences in the standard system.

STAR	α(2000)	δ(2000)	u (mag)	g (mag)	r (mag)	i (mag)	B (mag)	V (mag)	Y (mag)	J (mag)	H (mag)
						SN 2006V					
01	11:31:37.71	−02:18:48.30	. . .	. . .	. . .	. . .	. . .	. . .	12.444(006)	12.163(006)	11.800(006)
02	11:31:21.53	−02:20:22.56	17.469(072)	15.625(011)	14.923(011)	14.669(011)	16.091(009)	15.227(010)	. . .	. . .	. . .
03	11:31:45.09	−02:17:18.60	17.312(018)	16.154(011)	15.723(011)	15.570(011)	16.494(009)	15.900(008)	14.977(006)	14.715(006)	14.379(006)
04	11:31:20.58	−02:18:32.81	17.503(013)	16.226(013)	15.789(011)	15.643(011)	16.588(009)	15.963(008)	. . .	. . .	. . .
05	11:31:38.33	−02:21:37.42	18.270(026)	16.697(011)	16.089(011)	15.876(013)	17.130(011)	16.334(010)	15.172(009)	14.863(008)	14.434(007)
06	11:31:32.71	−02:21:53.30	19.600(084)	17.251(012)	16.221(018)	15.854(011)	17.819(011)	16.686(010)	14.980(009)	14.583(009)	14.014(009)
07	11:31:41.76	−02:16:13.31	19.153(052)	17.342(009)	16.564(010)	16.251(010)	17.837(009)	16.900(008)	15.450(006)	15.079(008)	14.584(008)
08	11:31:26.83	−02:19:17.16	20.471(180)	18.008(009)	16.735(011)	16.181(009)	18.673(012)	17.310(008)	15.257(079)	14.963(147)	14.301(130)
09	11:31:45.74	−02:19:25.57	. . .	18.437(009)	17.035(012)	15.927(010)	19.252(018)	17.638(008)	14.585(007)	14.108(008)	13.582(006)
10	11:31:32.39	−02:15:16.22	19.956(126)	18.008(009)	17.156(011)	16.824(009)	18.532(010)	17.547(008)	. . .	. . .	. . .
11	11:31:45.57	−02:16:45.48	18.951(055)	18.048(012)	17.753(009)	17.629(013)	18.296(014)	17.869(008)	17.100(017)	16.828(019)	16.554(034)
12	11:31:47.18	−02:21:27.35	. . .	19.166(029)	17.843(011)	17.176(013)	19.931(040)	18.446(011)	. . .	. . .	. . .
13	11:31:28.90	−02:17:16.32	20.975(281)	19.186(015)	17.980(019)	17.449(009)	19.813(026)	18.536(014)	16.487(010)	16.086(054)	15.480(054)
14	11:31:36.82	−02:19:57.30	. . .	19.102(023)	17.975(015)	17.489(009)	19.726(041)	18.498(009)	16.510(016)	16.078(009)	15.480(016)
15	11:31:29.08	−02:14:38.58	20.088(108)	18.906(020)	18.367(009)	18.169(010)	19.284(017)	18.601(013)	. . .	. . .	. . .
16	11:31:36.40	−02:18:16.45	19.388(265)	18.913(013)	18.429(012)	18.229(011)	19.280(031)	18.611(017)	. . .	. . .	. . .
17	11:31:26.40	−02:20:05.83	. . .	20.004(024)	18.559(027)	17.090(017)	20.856(075)	19.157(023)	. . .	. . .	. . .
18	11:31:43.91	−02:18:40.94	20.305(132)	19.117(015)	18.576(009)	18.365(013)	19.514(027)	18.775(021)	17.652(045)	17.326(046)	17.029(061)
19	11:31:37.16	−02:14:50.08	. . .	19.659(018)	18.669(027)	18.334(011)	20.176(060)	19.116(038)	. . .	. . .	. . .
20	11:31:25.90	−02:20:41.30	20.213(116)	19.340(014)	18.950(012)	18.775(026)	19.606(032)	19.074(015)	. . .	. . .	. . .
21	11:31:28.66	−02:19:25.59	20.534(180)	19.626(031)	19.279(020)	19.190(023)	19.902(030)	19.407(019)	. . .	. . .	. . .
22	11:31:42.41	−02:22:43.86	. . .	. . .	. . .	. . .	. . .	. . .	14.232(009)	13.925(009)	13.529(009)
23	11:31:49.73	−02:14:25.94	. . .	. . .	. . .	. . .	. . .	. . .	14.747(073)	14.604(062)	14.445(054)
24	11:31:54.45	−02:22:18.01	. . .	. . .	. . .	. . .	. . .	. . .	15.653(016)	15.177(009)	14.676(009)
25	11:31:55.23	−02:17:25.15	. . .	. . .	. . .	. . .	. . .	. . .	15.629(007)	15.200(006)	14.647(006)
26	11:31:30.39	−02:14:03.77	. . .	. . .	. . .	. . .	. . .	. . .	15.998(009)	15.494(011)	14.994(017)
27	11:31:46.96	−02:22:02.93	. . .	. . .	. . .	. . .	. . .	. . .	16.188(013)	15.690(013)	15.049(019)
28	11:31:29.32	−02:18:19.33	. . .	. . .	. . .	. . .	. . .	. . .	16.507(043)	16.020(074)	15.513(075)
29	11:31:49.54	−02:23:03.84	. . .	. . .	. . .	. . .	. . .	. . .	16.775(019)	16.229(021)	15.691(040)
30	11:31:49.62	−02:16:20.46	. . .	. . .	. . .	. . .	. . .	. . .	16.948(014)	16.426(015)	15.834(021)
31	11:31:27.00	−02:19:43.97	. . .	. . .	. . .	. . .	. . .	. . .	17.058(015)	16.625(081)	15.985(025)
32	11:31:27.36	−02:22:40.51	. . .	. . .	. . .	. . .	. . .	. . .	17.038(031)	16.585(021)	15.955(037)
33	11:31:57.32	−02:21:26.93	. . .	. . .	. . .	. . .	. . .	. . .	17.339(033)	16.959(033)	16.270(032)
34	11:31:34.96	−02:18:01.44	. . .	. . .	. . .	. . .	. . .	. . .	17.382(014)	16.964(015)	16.408(049)
35	11:31:55.07	−02:15:07.24	. . .	. . .	. . .	. . .	. . .	. . .	17.237(024)	16.770(024)	16.189(039)
36	11:31:35.43	−02:18:29.34	. . .	. . .	. . .	. . .	. . .	. . .	17.526(027)	17.067(083)	16.451(041)
37	11:31:31.01	−02:23:37.25	. . .	. . .	. . .	. . .	. . .	. . .	17.390(030)	16.993(040)	16.377(060)
38	11:31:31.89	−02:14:27.20	. . .	. . .	. . .	. . .	. . .	. . .	17.884(042)	17.501(059)	16.945(065)
39	11:31:51.38	−02:18:15.59	. . .	. . .	. . .	. . .	. . .	. . .	15.977(010)	15.492(007)	14.990(008)
40	11:31:41.17	−02:17:06.90	. . .	. . .	. . .	. . .	. . .	. . .	18.347(054)	17.917(050)	17.474(094)
						SN 2006au					
01	17:57:01.27	+12:12:17.97	. . .	. . .	. . .	. . .	. . .	. . .	. . .	. . .	. . .
02	17:57:26.02	+12:09:44.36	. . .	. . .	. . .	. . .	. . .	. . .	12.676(006)	12.432(006)	12.153(009)
03	17:57:25.34	+12:10:46.35	. . .	. . .	. . .	. . .	15.090(012)	. . .	. . .	. . .	. . .
04	17:57:24.92	+12:07:12.78	. . .	. . .	. . .	. . .	. . .	. . .	. . .	. . .	. . .
05	17:57:23.47	+12:13:48.50	. . .	. . .	. . .	. . .	. . .	. . .	. . .	. . .	. . .
06	17:57:21.28	+12:11:19.12	. . .	. . .	. . .	. . .	. . .	. . .	11.928(006)	11.703(009)	11.416(009)

Table 1 (cont'd)

STAR	α(2000)	δ(2000)	u (mag)	g (mag)	r (mag)	i (mag)	B (mag)	V (mag)	Y (mag)	J (mag)	H (mag)
07	17:57:21.20	+12:13:47.45	16.051(016)	14.925(015)	14.566(015)	14.447(015)	15.203(016)	14.664(035)	13.745(011)	13.557(012)	13.344(037)
08	17:57:20.99	+12:08:56.40	16.373(018)	...	...	...	15.212(009)	14.471(014)	13.325(006)	13.070(006)	12.773(009)
09	17:57:19.13	+12:12:49.98	...	...	...	...	...	...	...	...	...
10	17:57:14.53	+12:11:56.61	...	...	...	...	...	...	...	...	...
11	17:57:10.92	+12:14:24.91	...	...	...	...	...	...	...	...	...
12	17:57:10.72	+12:12:45.99	...	...	...	...	...	...	11.684(006)	11.384(020)	10.956(020)
13	17:57:10.58	+12:12:10.49	17.710(026)	15.397(015)	14.531(015)	14.210(015)	15.962(007)	14.884(010)	13.311(007)	12.961(013)	12.471(012)
14	17:57:07.66	+12:10:05.07	17.735(026)	...	...	...	15.698(008)	...	...	...	...
15	17:57:07.08	+12:12:04.19	...	...	...	...	...	...	...	...	...
16	17:57:24.01	+12:09:27.97	18.151(035)	15.910(009)	15.040(009)	14.698(013)	16.497(007)	15.399(008)	...	...	...
17	17:57:07.13	+12:12:39.82	17.220(017)	15.637(009)	15.060(009)	14.838(011)	16.075(007)	15.286(006)	...	...	...
18	17:57:10.34	+12:10:10.92	19.088(082)	16.416(007)	15.260(007)	14.789(009)	17.034(007)	15.780(007)	13.809(007)	13.421(014)	12.828(035)
19	17:57:04.06	+12:10:21.84	17.593(023)	16.090(007)	15.519(007)	15.292(007)	16.512(007)	15.743(006)	...	...	...
20	17:57:05.77	+12:07:10.60	18.015(061)	16.248(007)	15.532(007)	15.223(007)	16.723(008)	15.818(007)	...	...	...
21	17:57:05.24	+12:08:46.35	18.154(038)	16.294(007)	15.544(007)	15.218(007)	16.817(007)	15.848(006)	...	...	...
22	17:57:08.21	+12:08:23.53	18.508(049)	16.707(007)	16.046(007)	15.798(007)	17.176(009)	16.315(006)	...	...	...
23	17:57:26.13	+12:12:18.72	19.005(077)	16.967(007)	16.136(007)	15.781(008)	17.508(008)	16.476(006)	...	...	...
24	17:57:18.41	+12:11:17.41	19.073(129)	17.004(007)	16.213(007)	15.890(007)	17.545(008)	16.541(006)	15.038(008)	14.684(013)	14.193(013)
25	17:57:18.10	+12:07:34.41	19.381(114)	17.338(008)	16.478(007)	16.094(008)	17.881(012)	16.847(008)	...	...	...
26	17:57:17.76	+12:08:23.45	18.382(071)	17.006(007)	16.482(007)	16.277(009)	17.407(008)	16.693(006)	...	...	...
27	17:57:04.64	+12:11:26.91	18.523(052)	17.182(008)	16.620(007)	16.377(007)	17.579(009)	16.850(007)	...	...	...
28	17:57:10.82	+12:08:44.31	18.985(078)	17.505(007)	16.955(007)	16.745(011)	17.922(009)	17.171(006)	16.010(006)	15.737(007)	15.393(022)
29	17:57:24.06	+12:08:07.25	19.253(099)	17.641(007)	17.075(007)	16.850(007)	18.080(010)	17.291(007)	...	...	...
30	17:57:39.05	+12:08:46.21	...	...	...	...	...	...	15.015(007)	14.646(007)	14.172(013)
31	17:57:23.88	+12:11:39.48	...	...	...	...	...	...	16.760(014)	16.507(013)	16.237(047)
32	17:57:29.01	+12:11:17.38	...	...	...	...	...	...	16.880(014)	16.589(016)	16.261(043)
33	17:57:34.21	+12:12:06.84	...	...	...	...	...	...	16.879(013)	16.579(014)	16.204(033)
34	17:57:13.41	+12:07:53.58	...	...	...	...	...	...	17.032(025)	16.706(041)	16.217(070)
35	17:57:40.05	+12:13:03.83	...	...	...	...	...	...	17.056(015)	16.747(029)	16.345(065)
36	17:57:10.67	+12:09:20.38	...	...	...	...	...	...	17.090(016)	16.722(015)	16.294(048)
37	17:57:22.71	+12:09:52.74	...	...	...	...	...	...	17.127(025)	16.656(020)	16.096(038)
38	17:57:40.25	+12:09:44.53	...	...	...	...	...	...	17.099(028)	16.746(020)	16.270(054)
39	17:57:14.91	+12:13:28.13	...	...	...	...	...	...	17.578(045)	17.153(032)	16.523(157)
40	17:57:16.09	+12:12:23.22	...	...	...	...	...	...	17.656(039)	17.261(024)	16.621(038)
41	17:57:20.72	+12:07:54.01	...	...	...	...	...	...	17.803(050)	17.314(039)	16.852(063)
42	17:57:14.90	+12:11:26.23	...	...	...	...	...	...	14.535(007)	14.045(012)	13.428(007)
43	17:57:12.58	+12:11:23.64	...	...	...	...	...	...	17.510(024)	17.171(024)	16.558(031)
44	17:57:16.80	+12:11:22.09	...	...	...	...	...	...	16.658(013)	16.329(021)	15.807(022)
45	17:57:10.85	+12:11:15.14	...	...	...	...	...	...	16.649(027)	16.364(041)	15.994(061)
46	17:57:16.99	+12:11:49.88	...	...	...	...	...	...	17.242(019)	16.910(016)	16.380(031)
47	17:57:12.86	+12:09:42.55	...	...	...	...	...	...	16.118(014)	15.815(016)	15.401(023)
48	17:57:18.86	+12:12:19.19	...	...	...	...	...	...	16.814(010)	16.563(018)	16.178(029)
49	17:57:17.80	+12:10:20.24	...	...	...	...	...	...	16.227(010)	15.801(013)	15.130(015)
50	17:57:22.52	+12:10:57.65	...	...	...	...	...	...	16.196(009)	15.736(007)	15.211(014)

Note. — Uncertainties given in parentheses in thousandths of a magnitude correspond to an rms of the magnitudes obtained on photometric nights.

Table 2. Spectroscopic observations of SN 2006V and SN 2006au.

Date (UT)	Julian Date JD - 2,453,000	Epoch[a] (days)	Telescope	Instrument	Range (Å)	Resolution (FWHM Å)	Integration (sec)
SN 2006V							
2006 Feb. 13	779.8	−43.9	NTT	EMMI	4000 − 10200	9	300
2006 Mar. 05	799.8	−23.8	Du Pont	WFCCD	3800 − 9235	8	900
2006 Mar. 08	802.8	−20.9	Du Pont	WFCCD	3800 − 9235	8	900
2006 Mar. 15	809.8	−13.8	Clay	LDSS	3785 − 9969	2-4[b]	600
2006 Mar. 23	817.7	−6.0	Du Pont	WFCCD	3800 − 9235	8	900
2006 Mar. 24	818.8	−4.9	Du Pont	WFCCD	3800 − 9235	8	900
2006 Apr. 02	827.7	+4.0	Du Pont	WFCCD	3800 − 9235	8	900
2006 Apr. 16	841.7	+18.0	Baade	IMACS	3842 − 9692	4	900
2006 Apr. 24	849.6	+25.9	Du Pont	WFCCD	3800 − 9235	8	900
SN 2006au							
2006 Mar. 14	808.9	−56.6	Clay	LDSS	3785 − 9969	2-4[b]	600
2006 Mar. 15	809.9	−55.6	NTT	EMMI	4000 − 10200	8	300
2006 Mar. 22	816.9	−48.6	Du Pont	WFCCD	3800 − 9235	8	600
2006 Mar. 23	817.9	−47.6	Du Pont	WFCCD	3800 − 9235	8	900
2006 Mar. 24	818.9	−46.6	Du Pont	WFCCD	3800 − 9235	8	600
2006 Mar. 30	824.9	−40.6	Du Pont	WFCCD	3800 − 9235	8	900
2006 Apr. 02	827.9	−37.6	Du Pont	WFCCD	3800 − 9235	8	600
2006 Apr. 22	847.8	−17.7	Du Pont	WFCCD	3800 − 9235	8	600
2006 Apr. 25	850.9	−14.6	Du Pont	WFCCD	3800 − 9235	8	600

[a]Days since $B_{\max}$.

[b]The spectrum was obtained by the combination of two spectra from two different grisms, respectively covering the range between 3785 and 6129 Å and the one between 5673 and 9969 Å. The resolutions were different, being 2 Å on the blue side and 4 Å on the red one.

Table 3. Photometric observations of SN 2006V in the optical filters.

JD - 2, 453, 000	Phase[a]	u (mag)	g (mag)	r (mag)	i (mag)	B (mag)	V (mag)	Instrument
771.17	−52.53	...	...	18.0[b]	...	...	...	LOT CCD
773.15	−50.55	...	...	18.2[b]	...	...	...	LOT CCD
773.71	−49.99	21.933(492)	18.724(012)	18.076(009)	18.021(011)	19.306(024)	18.355(012)	Site 3
774.82	−48.88	21.454(231)	18.712(011)	18.042(009)	17.980(011)	19.209(020)	18.305(012)	Site 3
775.67	−48.03	21.059(191)	18.684(010)	18.002(009)	17.949(011)	19.171(020)	18.267(010)	Site 3
778.81	−44.89	21.082(321)	18.546(019)	17.890(016)	17.825(015)	19.034(039)	18.128(019)	Site 3
784.90	−38.80	19.858(380)	...	...	...	18.912(050)	17.956(016)	Site 3
786.88	−36.82	20.559(218)	18.302(011)	17.657(009)	17.610(010)	18.772(021)	17.890(011)	Site 3
795.84	−27.86	...	18.092(006)	17.455(007)	17.414(008)	18.613(013)	17.701(007)	Site 3
799.75	−23.95	...	17.999(006)	17.374(006)	17.344(007)	18.537(011)	17.616(006)	Site 3
804.84	−18.86	...	17.916(006)	17.291(005)	17.252(006)	18.435(009)	17.532(007)	Site 3
805.79	−17.91	...	17.901(007)	17.282(007)	17.239(008)	18.405(013)	17.531(008)	Site 3
818.77	−4.93	...	17.769(009)	17.135(008)	17.096(009)	18.287(013)	17.388(009)	Site 3
824.73	+1.03	...	17.749(006)	17.106(006)	17.059(006)	18.291(009)	17.351(006)	Site 3
832.75	+9.05	...	17.813(006)	17.130(007)	17.071(008)	18.344(010)	17.391(007)	Site 3
838.75	+15.05	...	17.942(016)	17.205(009)	17.144(010)	18.458(041)	17.499(014)	Site 3
846.73	+23.03	...	18.258(008)	17.430(006)	17.339(008)	18.888(014)	17.787(007)	Site 3
853.64	+29.94	...	18.752(009)	17.795(008)	17.664(009)	19.426(018)	18.219(009)	Site 3
862.57	+38.87	...	19.263(016)	18.186(010)	18.041(012)	19.950(030)	18.676(014)	Site 3
867.57	+43.87	...	19.337(029)	18.278(012)	18.143(017)	20.174(086)	18.757(026)	Site 3
892.56	+68.86	...	19.697(026)	18.518(018)	18.443(024)	...	19.052(048)	Tek 5
898.56	+74.86	...	19.759(020)	18.567(015)	18.500(021)	20.468(034)	19.213(018)	Tek 5

Note. — Values in parentheses are 1σ measurement uncertainties in 10^{-3} of mag.

[a]Days since B_{max}, $JD = 2453823.7$.

[b]Unfiltered magnitudes from discovery and confirmation images, obtained with the Lulin One-meter Telescope (LOT) in Taiwan (Chen et al. 2006).

Table 4. Photometric observations of SN 2006V in the NIR filters.

JD - 2, 453, 000	Phase[a]	Y (mag)	J (mag)	H (mag)	Instrument
777.78	−45.92	17.306(029)	17.053(048)	16.919(063)	Retrocam
779.79	−43.91	17.283(038)	17.002(039)	16.819(062)	Retrocam
788.86	−34.84	17.059(012)	16.862(018)	16.713(027)	WIRC
797.75	−25.95	16.994(035)	16.659(035)	16.502(056)	RetroCam
803.84	−19.86	16.767(027)	...	...	RetroCam
810.79	−12.91	16.648(024)	16.450(030)	16.245(047)	RetroCam
817.71	−5.99	16.600(027)	16.361(026)	16.087(024)	RetroCam
826.68	+2.98	16.538(019)	16.275(020)	16.096(031)	RetroCam
834.74	+11.04	16.569(010)	16.343(016)	16.193(030)	WIRC
844.65	+20.95	16.723(012)	16.514(039)	16.261(026)	WIRC
852.64	+28.94	16.971(027)	16.692(035)	16.450(056)	RetroCam
863.59	+39.89	17.261(050)	17.148(063)	...	RetroCam
869.64	+45.94	17.428(038)	17.209(048)	16.853(061)	RetroCam

Note. — Values in parentheses are 1σ measurement uncertainties in 10^{-3} of mag.

[a]Days since B_{max}, $JD = 2453823.7$.

Table 5. Photometric observations of SN 2006au in the optical filters.

JD - 2, 453, 000	Phase[a]	u (mag)	g (mag)	r (mag)	i (mag)	B (mag)	V (mag)	Instrument
801.70	−63.80	. . .	. . .	17.2[b]	. . .	. . .	. . .	AP-7 CCD
805.15	−60.35	. . .	. . .	17.4[b]	. . .	. . .	. . .	AP-7 CCD
805.89	−59.61	20.609(210)	18.428(015)	17.614(027)	17.106(093)	19.079(018)	17.991(013)	Site 3
809.85	−55.65	. . .	18.366(027)	17.589(028)	17.327(026)	19.308(065)	17.963(020)	Site 3
815.86	−49.64	20.815(198)	18.468(024)	17.696(051)	17.388(039)	19.206(027)	18.061(024)	Site 3
818.90	−46.60	20.446(230)	18.563(016)	17.637(023)	17.335(028)	19.219(023)	18.079(019)	Site 3
819.90	−45.60	20.751(225)	18.578(022)	17.575(035)	. . .	19.244(020)	18.056(020)	Site 3
823.83	−41.67	20.123(287)	18.549(016)	17.604(024)	17.371(026)	19.144(018)	18.061(018)	Site 3
824.87	−40.63	20.448(226)	18.485(011)	17.557(016)	17.369(018)	19.149(019)	18.036(013)	Site 3
828.89	−36.61	20.555(265)	18.321(036)	. . .	. . .	19.054(010)	17.953(018)	Tek 5
829.92	−35.58	19.982(237)	18.542(038)	. . .	. . .	19.056(025)	. . .	Tek 5
830.89	−34.61	20.482(257)	. . .	17.463(071)	17.402(081)	19.011(013)	18.045(039)	Tek 5
831.83	−33.67	20.288(299)	18.304(018)	17.451(018)	17.362(025)	. . .	17.982(018)	Site 3
832.86	−32.64	20.389(297)	18.408(009)	. . .	. . .	18.992(015)	17.957(010)	Site 3
835.87	−29.63	20.285(282)	18.335(021)	17.501(037)	17.239(025)	18.923(016)	17.918(018)	Site 3
838.82	−26.68	20.291(314)	18.175(021)	17.376(024)	17.083(033)	18.775(040)	17.775(018)	Site 3
840.83	−24.67	20.185(224)	18.121(024)	17.376(025)	17.168(024)	18.796(029)	17.760(015)	Site 3
841.85	−23.65	19.820(225)	18.133(021)	17.341(029)	17.112(023)	18.788(026)	17.749(019)	Site 3
845.82	−19.68	. . .	18.096(012)	17.266(017)	17.043(019)	18.703(021)	17.666(012)	Site 3
850.81	−14.69	. . .	18.087(011)	17.222(017)	16.991(020)	18.720(014)	17.601(010)	Site 3
853.85	−11.65	. . .	18.056(016)	17.185(025)	16.974(023)	18.677(013)	17.598(016)	Site 3
858.79	−6.71	. . .	18.016(007)	17.105(006)	16.929(015)	18.649(020)	17.506(015)	Site 3
861.82	−3.68	. . .	18.006(016)	17.099(028)	16.867(023)	18.654(013)	17.535(016)	Site 3
862.80	−2.70	. . .	18.018(009)	17.084(008)	. . .	18.653(014)	17.509(009)	Site 3
866.75	+1.25	. . .	17.966(024)	16.996(031)	16.824(020)	18.628(021)	17.464(017)	Site 3
867.78	+2.28	. . .	17.978(029)	16.981(035)	16.866(035)	18.678(028)	17.491(024)	Site 3
870.80	+5.30	. . .	18.028(018)	17.013(018)	16.764(017)	18.675(034)	17.467(012)	Site 3
871.79	+6.29	. . .	18.031(017)	17.022(016)	16.799(018)	18.768(029)	17.486(015)	Site 3
872.78	+7.28	. . .	18.085(030)	16.994(043)	16.792(032)	18.776(022)	17.562(026)	Site 3
886.78	+21.28	. . .	. . .	. . .	17.049(059)	19.360(020)	18.041(041)	Tek 5
890.72	+25.22	. . .	18.832(026)	17.469(024)	17.258(025)	19.437(179)	18.127(063)	Site 3
891.74	+26.24	. . .	18.883(017)	17.551(023)	17.258(025)	19.692(026)	18.211(016)	Site 3
892.76	+27.26	. . .	18.987(064)	17.623(069)	17.353(054)	19.729(013)	18.212(024)	Tek 5
893.71	+28.21	. . .	19.097(073)	17.479(042)	17.305(044)	19.839(024)	18.299(016)	Tek 5
894.75	+29.25	. . .	. . .	17.669(017)	17.473(019)	19.854(035)	18.340(010)	Tek 5
897.66	+32.16	. . .	. . .	18.015(150)	. . .	20.477(095)	18.830(097)	Tek 5
898.71	+33.21	. . .	. . .	18.434(116)	. . .	21.185(231)	19.041(202)	Tek 5

Note. — Values in parentheses are 1σ measurement uncertainties in 10^{-3} of mag.

[a]Days since B_{max}, $JD = 2453865.5$.

[b]Unfiltered magnitudes from discovery and confirmation images, obtained with the 0.35 m Tenagra telescope in Oslo (Trondal et al. 2006).

Table 6. Photometric observations of SN 2006au in the NIR filters.

JD - 2, 453, 000	Phase[a]	Y (mag)	J (mag)	H (mag)	Instrument
807.87	−57.63	16.630(020)	16.398(025)	16.257(046)	RetroCam
808.85	−56.65	16.704(024)	16.375(027)	16.224(042)	RetroCam
810.87	−54.63	16.711(022)	16.377(020)	. . .	RetroCam
813.87	−51.63	16.645(021)	16.380(019)	. . .	RetroCam
820.87	−44.63	16.632(022)	16.371(018)	16.201(044)	RetroCam
826.83	−38.67	16.623(020)	16.366(022)	16.160(051)	RetroCam
834.87	−30.63	16.554(009)	16.248(009)	16.050(014)	WIRC
839.83	−25.67	16.456(019)	16.188(020)	16.050(040)	RetroCam
845.83	−19.67	16.353(008)	16.093(009)	15.838(013)	WIRC
848.83	−16.67	16.314(016)	16.052(016)	15.838(032)	RetroCam
868.80	+3.30	16.073(015)	15.794(011)	15.615(027)	RetroCam

Note. — Values in parentheses are 1σ measurement uncertainties in 10^{-3} of mag.

[a]Days since B_{max}, $JD = 2453865.5$.

Table 7.   Absolute peak magnitudes of SN 2006V and SN 2006au in both optical and NIR filters.

Filter	JD - 2, 453, 000	Phase[a]	Peak (mag)	JD - 2, 453, 000	Phase[a]	Peak (mag)
		SN 2006V			**SN 2006au**	
g	824.5	76.5	-16.67	866.9	72.9	-16.55
r	825.0	77.0	-17.28	867.5	73.5	-17.20
i	825.3	77.3	-17.31	868.5	74.5	-17.15
B	823.7	75.7	-16.14	865.5	71.5	-16.02
V	824.8	76.8	-17.05	867.0	73.0	-16.87
Y	825.5	77.5	-17.81	868.5	74.5	-17.63
J	825.8	77.8	-18.06	868.5	74.5	-17.81
H	823.7	75.7	-18.26	868.5	74.5	-17.90

Note. — The largest uncertainty affecting the absolute magnitudes is related to the distance estimate, whose error is about 7%.

[a]Days since explosion, $JD = 2453748$ for SN 2006V and $JD = 2453794$ for SN 2006au.

Table 8.   Physical parameters for BSG supernovae.

Parameter	SN 2006V	SN 2006au	SN 1987A	SN 1998A	SN 2000cb	SN 2009E
Explosion energy (10^{51} erg)	2.4	3.2	1.1	5.6	4.4	0.6
Ejecta mass ($M_\odot$)	17.0	19.3	11.8	22.0	22.3	19.0
Radius ($R_\odot$)	75	90	33	≤ 86	35	101
^{56}Ni mass ($M_\odot$)	0.127	≤ 0.073	0.078	0.11	0.083	0.039

Note. — SN 1998A data are from Pastorello et al. (2005), SN 2000cb from Utrobin & Chugai (2011) and SN 2009E from Pastorello et al. (2011). The parameters for our objects and SN 1987A have been obtained from the semi-analytic model explained in the text.
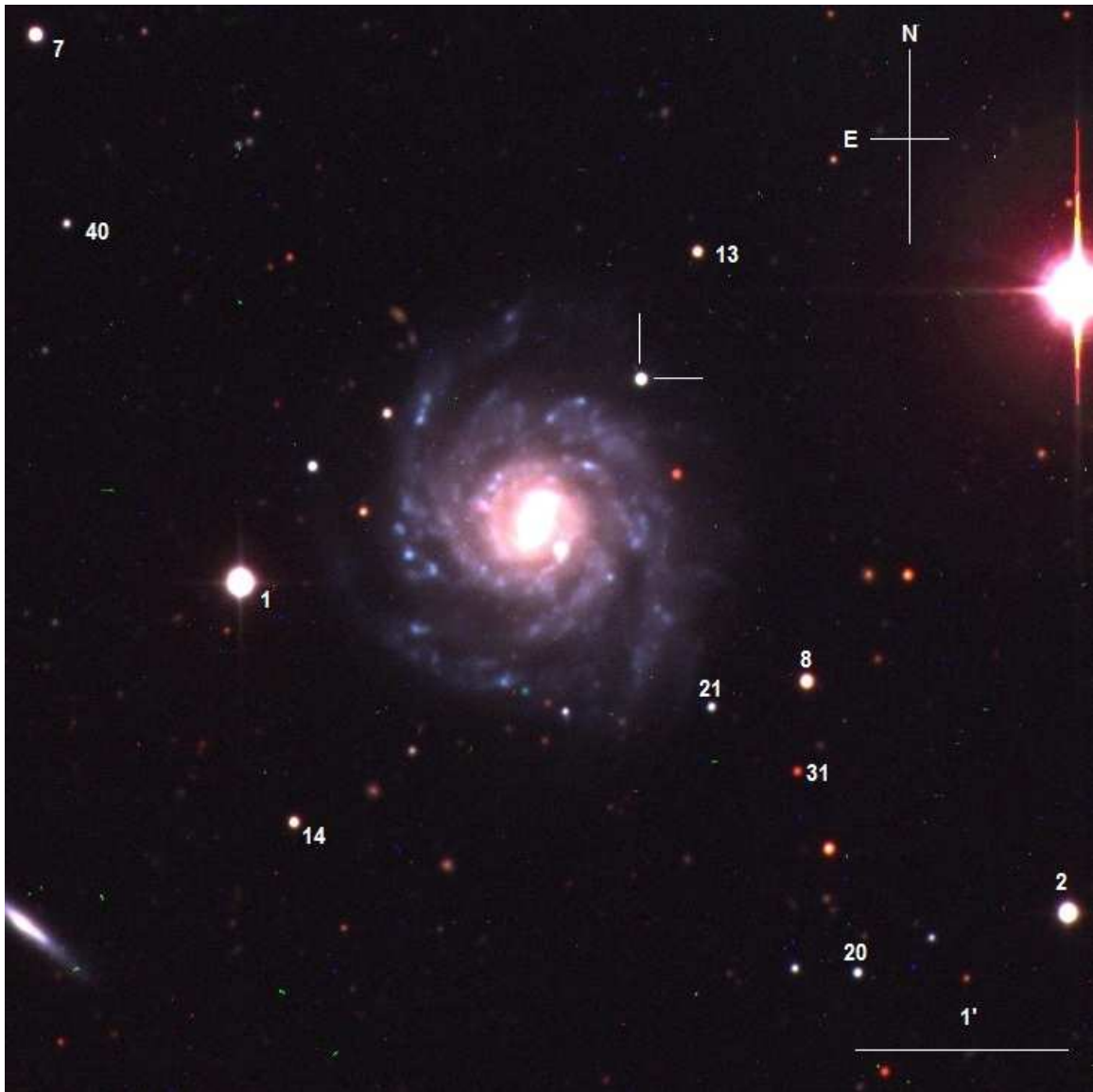
Figure 1: A composite optical image of UGC 6510 with the position of SN 2006V indicated, along with the orientation, the scale and some local sequence stars. The optical images were taken with the Swope telescope.
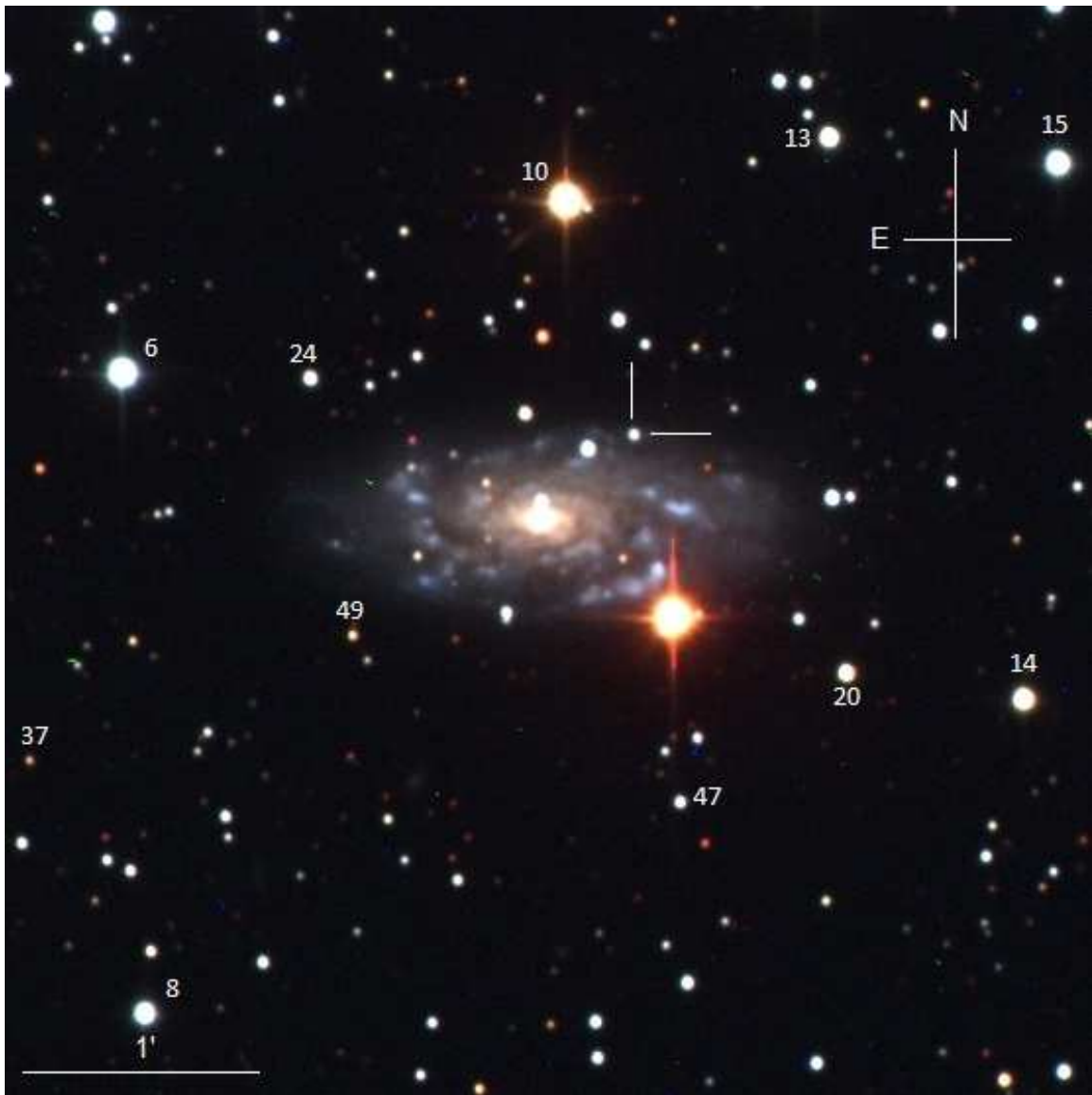
Figure 2: A composite optical image of UGC 11057 with the position of SN 2006au indicated, along with the orientation, the scale and some local sequence stars. The optical images were taken with the Swope telescope.
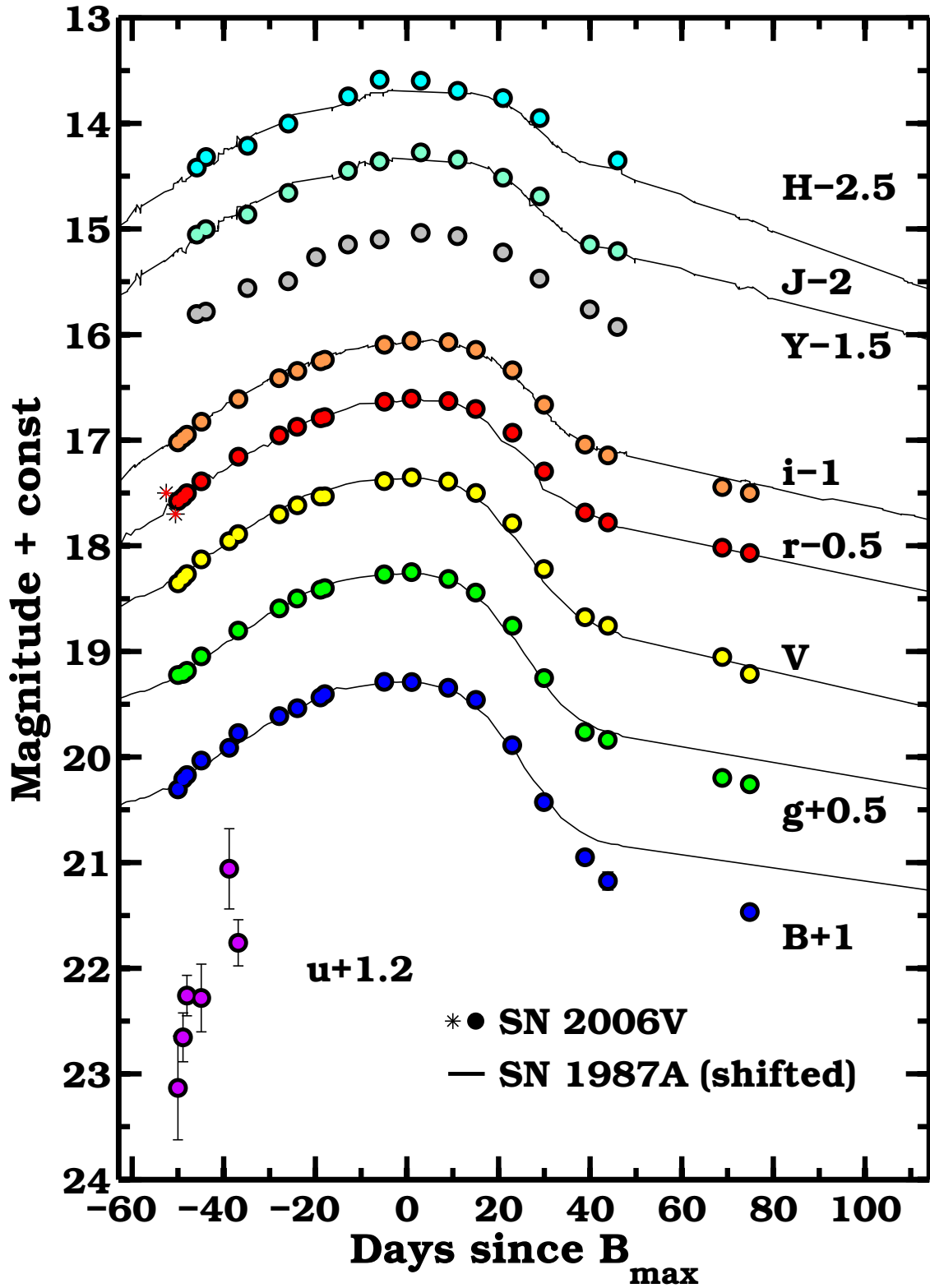
Figure 3: Optical and near-infrared light curves of SN 2006V. Over-plotted as solid lines are light curves of SN 1987A (J and H from Bouchet et al. 1989; I from Hamuy et al. 1988; $BgVr$ from spectrophotometry on the spectra sample published in Phillips et al. 1988) scaled to match the peak brightness of SN 2006V. We also show (stars) the unfiltered/r magnitudes from discovery and confirmation images (Chen et al. 2006). The similarity of the light curve shape of these two objects is striking.
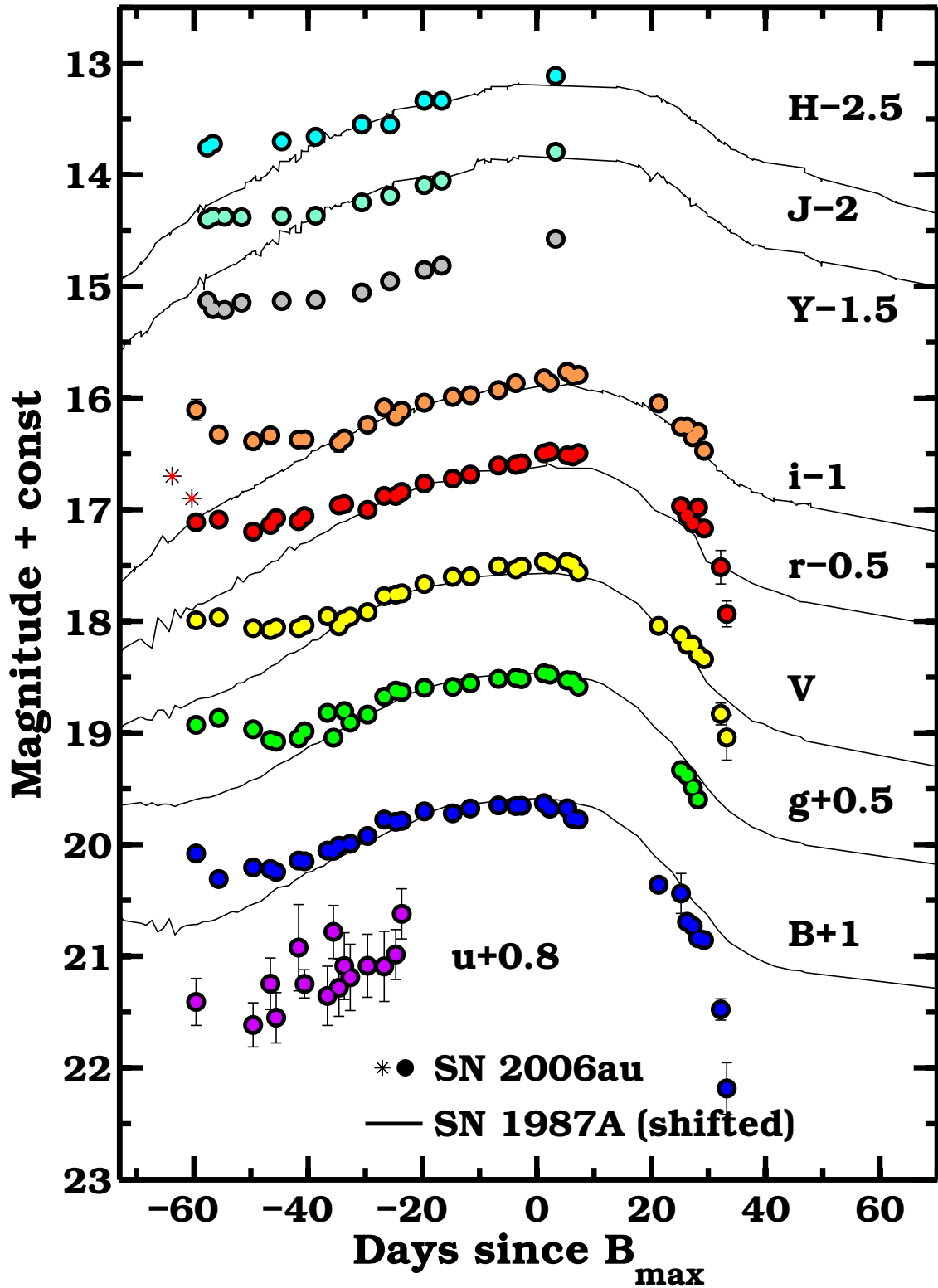
Figure 4: Optical and near-infrared light curves of SN 2006au. Over-plotted as solid lines are light curves of SN 1987A (J and H from Bouchet et al. 1989; I from Hamuy et al. 1988; $BgVr$ from spectrophotometry on the spectra sample published in Phillips et al. 1988) scaled to match the peak brightness of SN 2006au. We also show (stars) the unfiltered/r magnitudes from discovery and confirmation images (Trondal et al. 2006). The two objects have nearly identical evolution between -30 to $+30$ days past maximum. At earlier epochs SN 2006au shows evidence of the tail end of the cooling phase that followed shock break-out. At later epochs the B, V and r-band light curves of SN 2006au appear to drop at a faster rate.
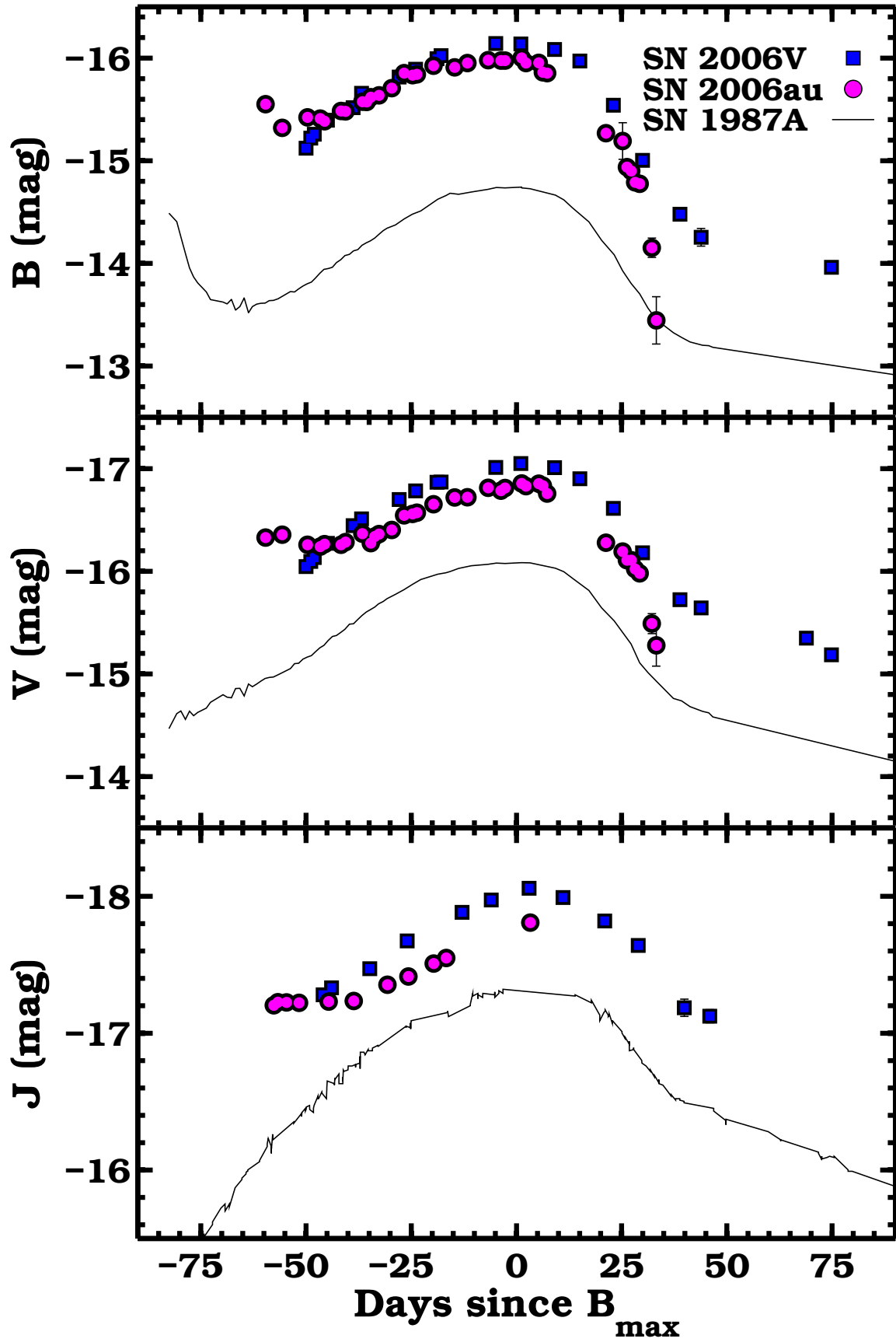
Figure 5: Absolute B (top panel), V (middle panel) and J (bottom panel) light curves of SNe 1987A (Hamuy et al. 1988), 2006V and 2006au. For SN 1987A we adopt $E(B-V)_{tot} = 0.175$ mag (Woosley et al. 1987) and a distance of $d = 50 \pm 5.2$ kpc (Storm et al. 2004).
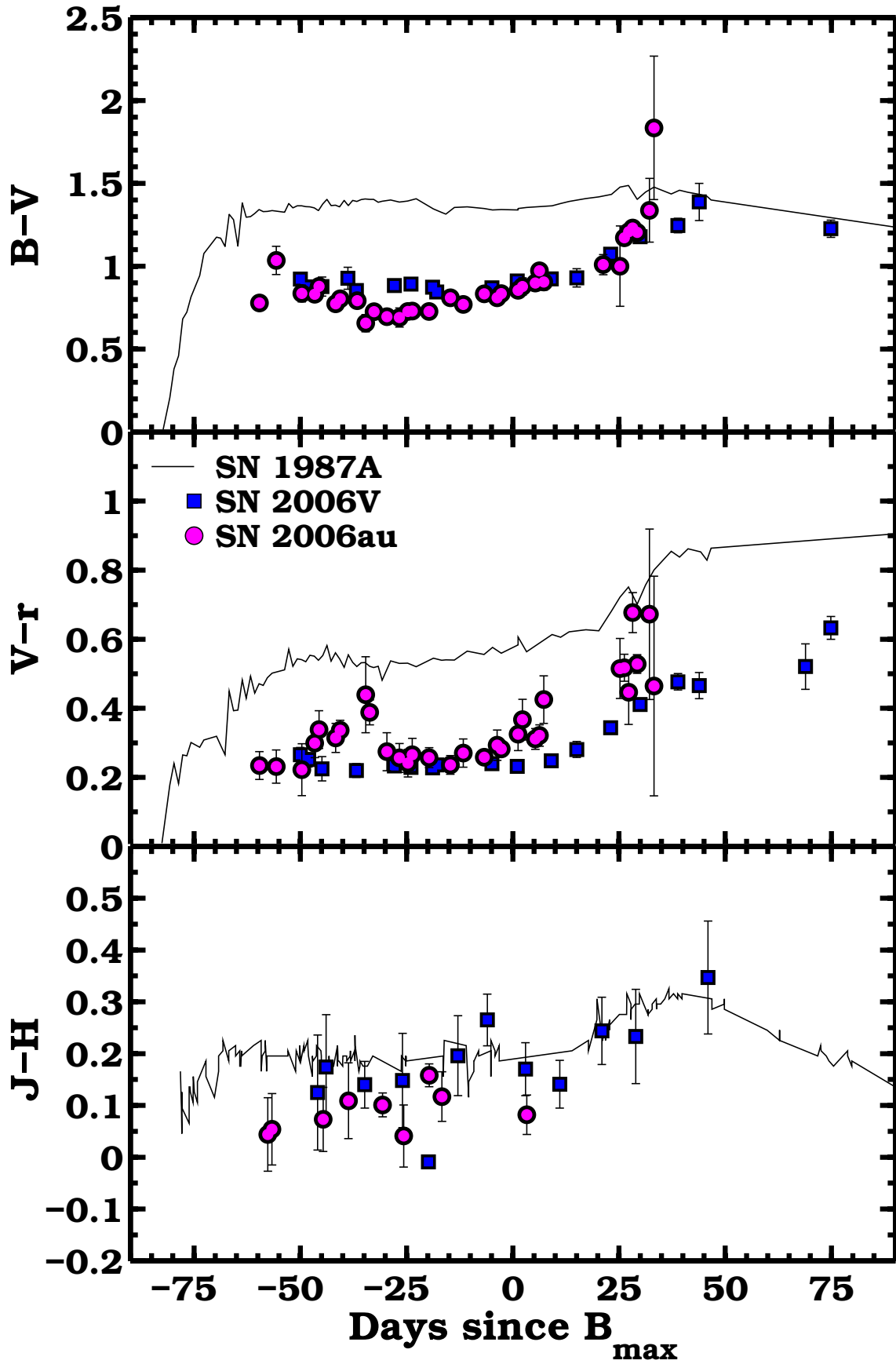
Figure 6: $B - V$ (top panel), $V - r$ (middle panel) and $J - H$ (bottom panel) color curves for SNe 2006V, 2006au, and 1987A. Both SNe 2006V and 2006au are considerably bluer than SN 1987A.
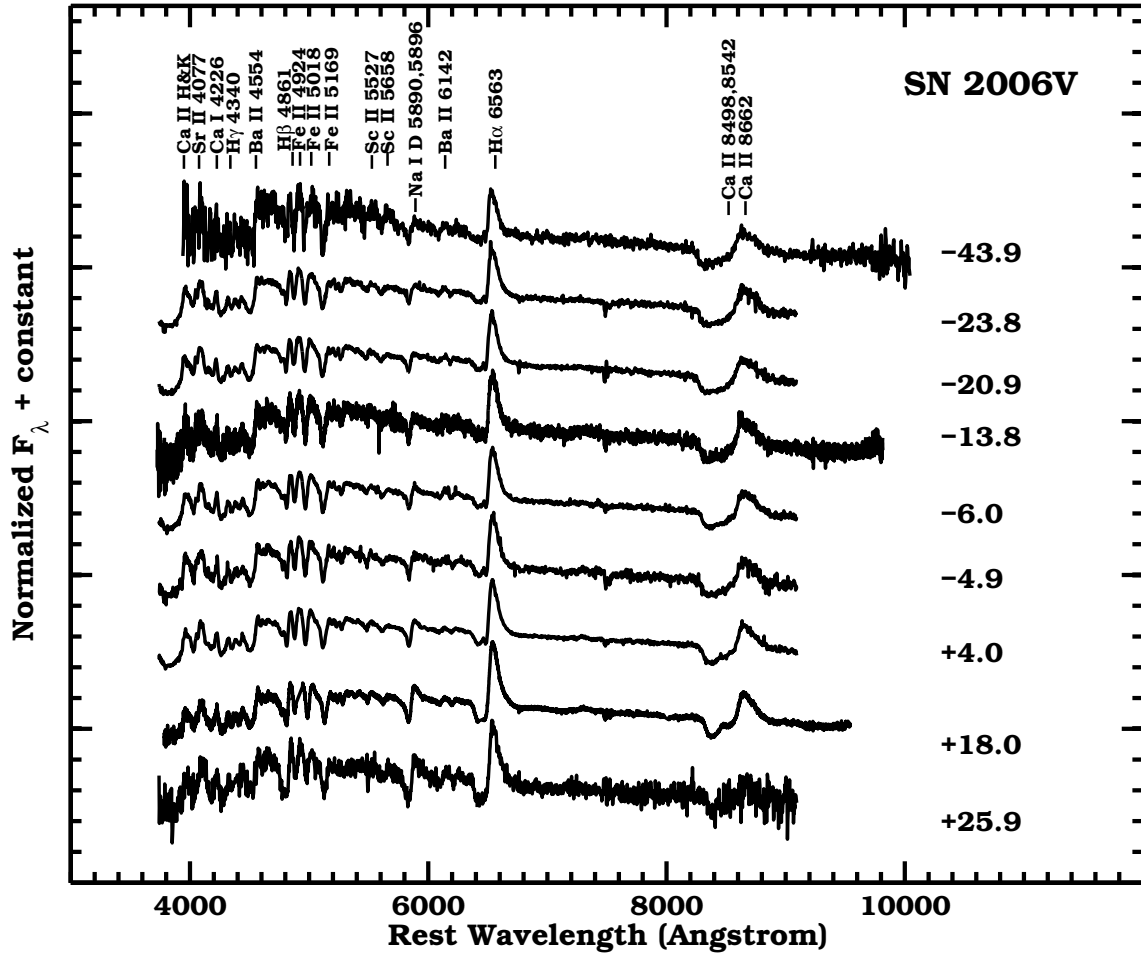
Figure 7: Spectral evolution of SN 2006V. Days since B_{max} are reported in the figure. The spectra exhibit strong Hα P-Cygni profiles, Fe II features and Na I, and are similar to those of normal SNe II.
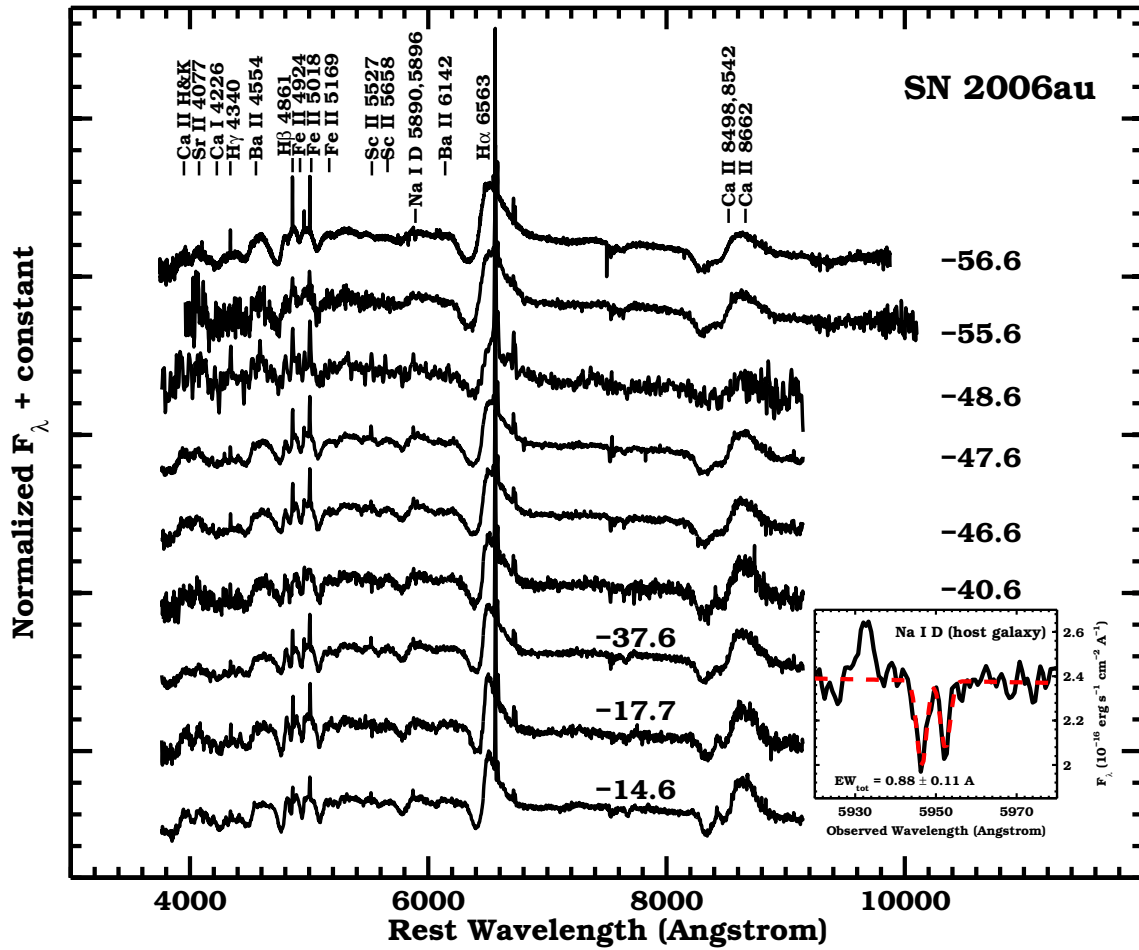
Figure 8: Spectral evolution of SN 2006au. Days since B_{max} are reported in the figure. Overall these spectra resemble those of SN 2006V. The narrow emission lines are from the host galaxy. Shown in the inset is the spectrum obtained on 14th March 2006 plotted in the rest frame of the host galaxy, in the wavelength range where narrow Na I D absorption feature has been detected. Over-plotted (red dashed line) is the best fit of two Gaussians with a FWHM of 2.8 Å, from which we obtain a total equivalent width of 0.88 ± 0.11 Å.
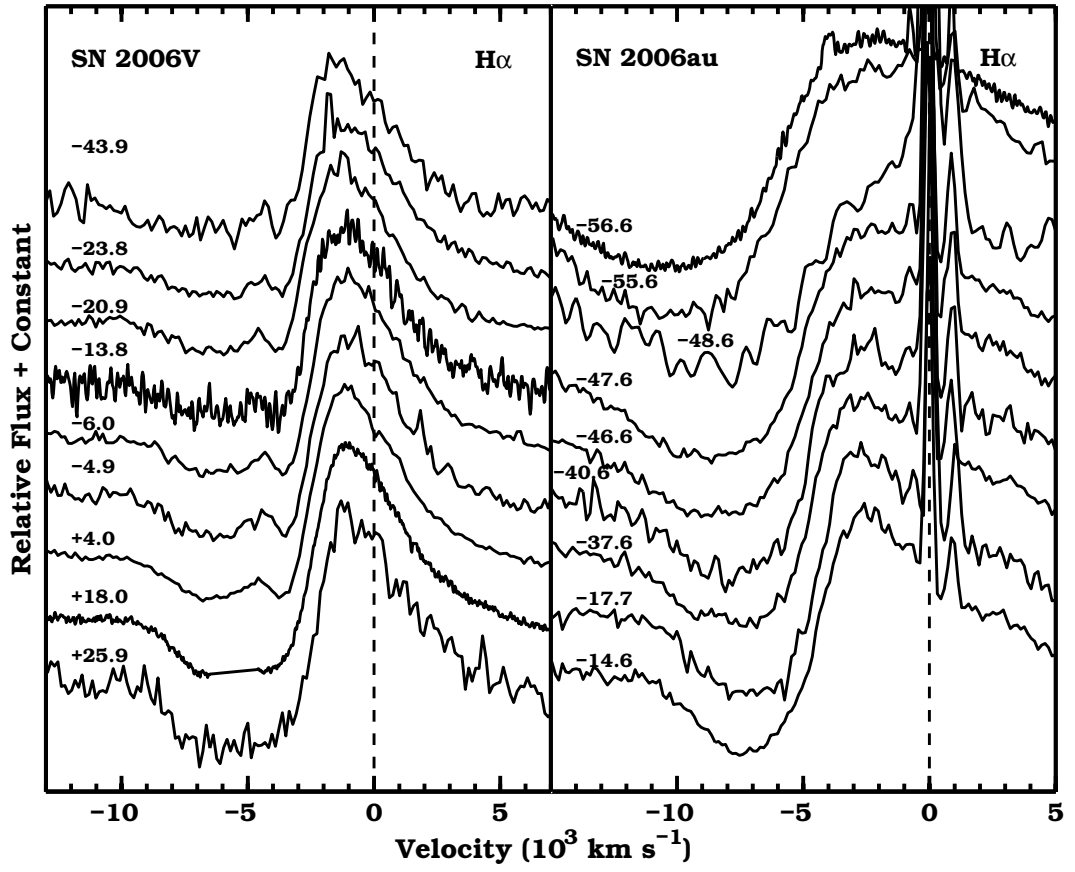
Figure 9: Hα P-Cygni profile evolution for SN 2006V (left panel) and SN 2006au (right panel). Since the spectra of SN 2006V are not particularly early (days since B_{max} are reported on the left), the velocity corresponding to the minimum of absorption is almost constant. For SN 2006au, the shift towards lower velocities in the last six spectra is evident.
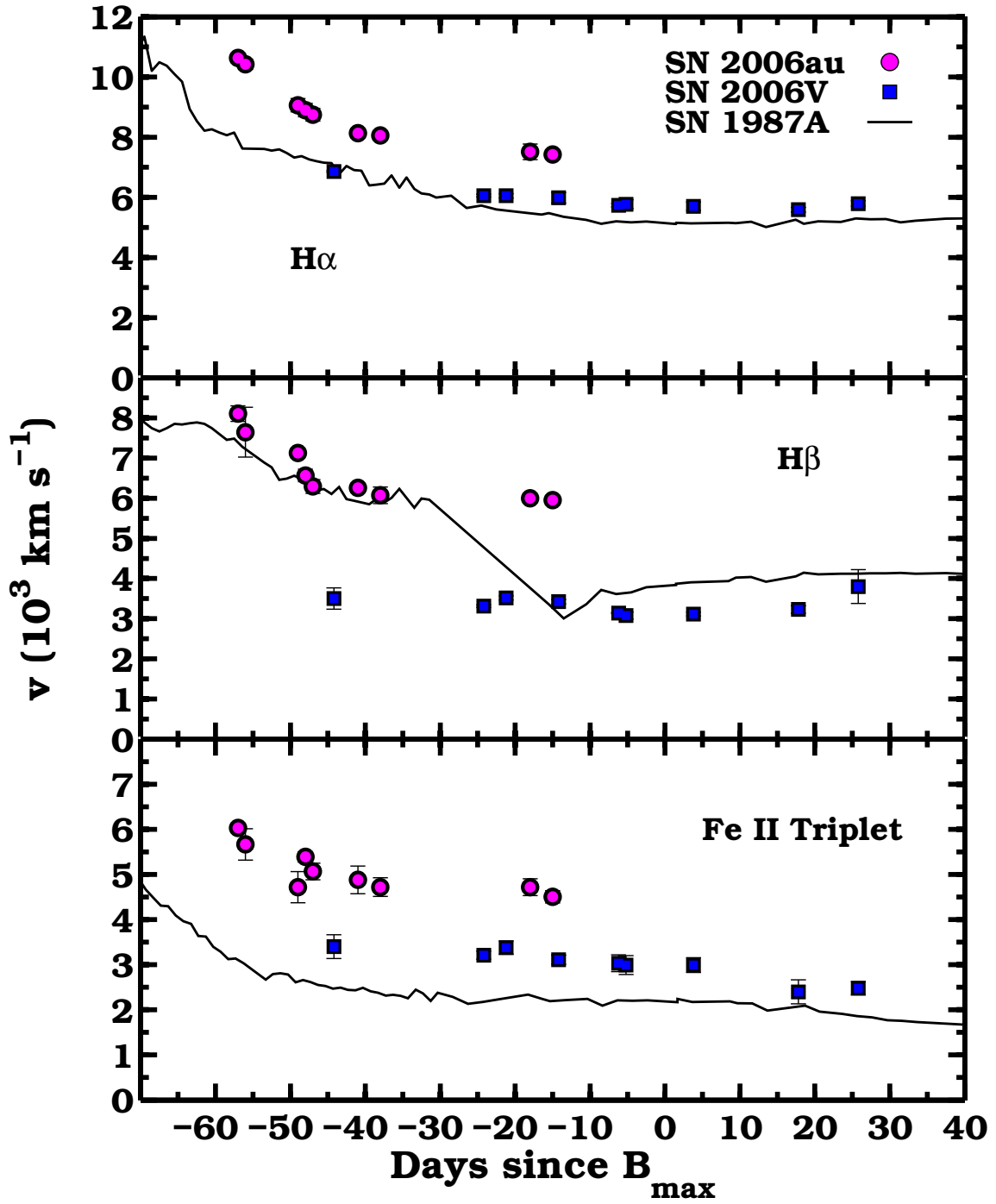
Figure 10: Measured expansion velocities for SNe 2006V, 2006au and 1987A, from the minimum of absorption of Hα (top panel), Hβ (middle panel) and Fe II multiplet 42 (bottom panel).
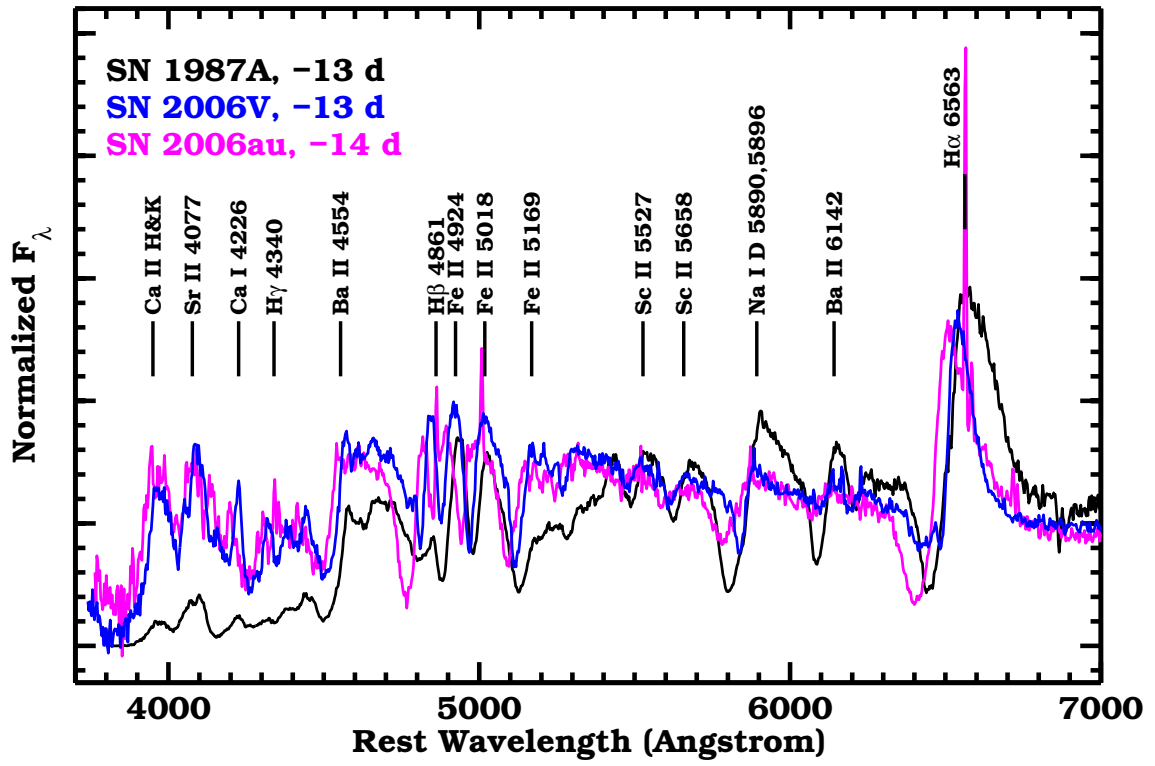
Figure 11: Optical spectral comparison of SNe 2006au, 2006V and 1987A, about two weeks before B_{max}. Both SNe 2006V and 2006au appear bluer, but the spectral features are comparable, although the intensities are different.
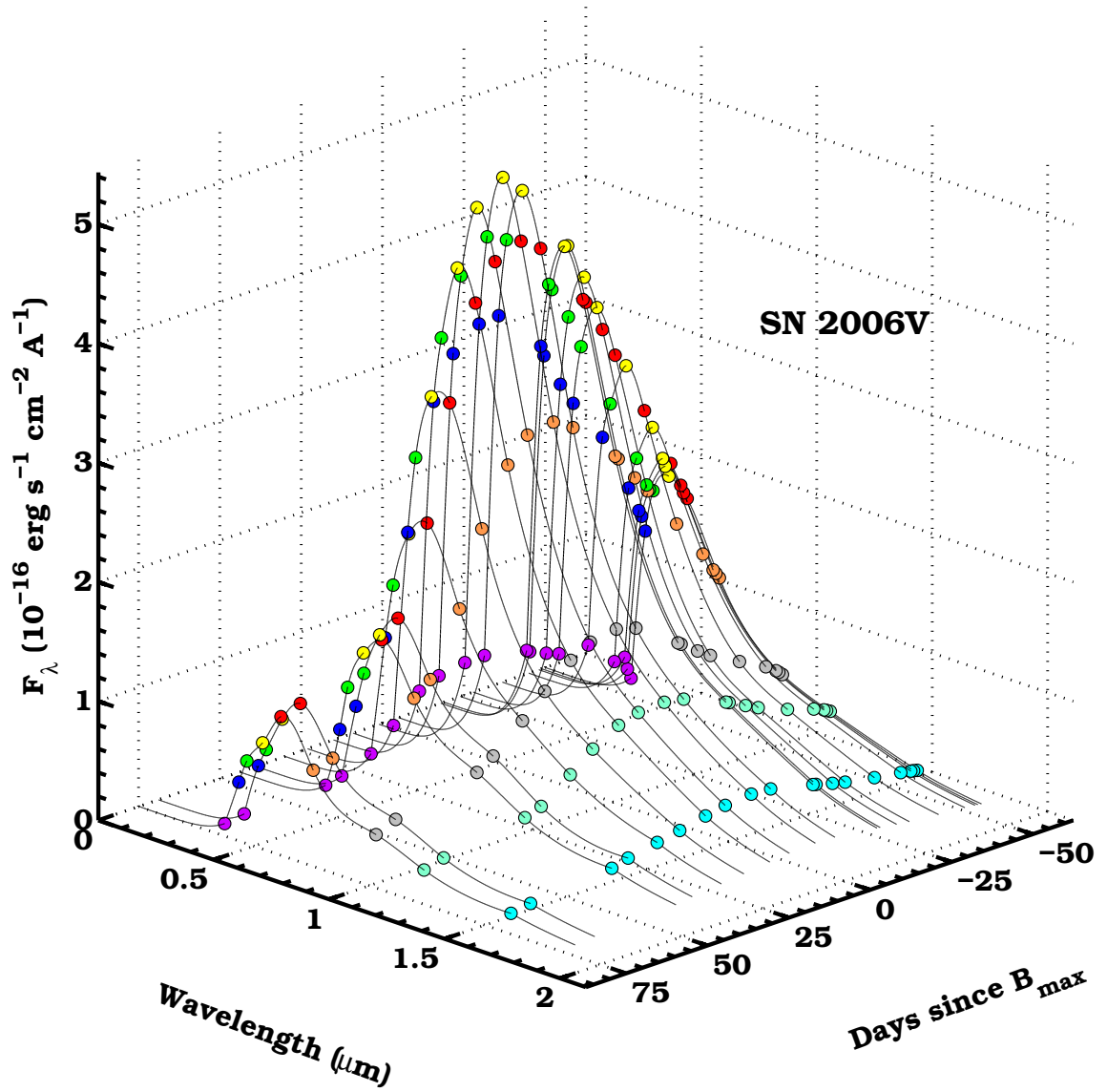
Figure 12: Spectral energy distributions as a function of time for SN 2006V. The colors correspond to those adopted for each band in Fig. 3. The spline fit along with the IR and UV tails are also shown (solid line).
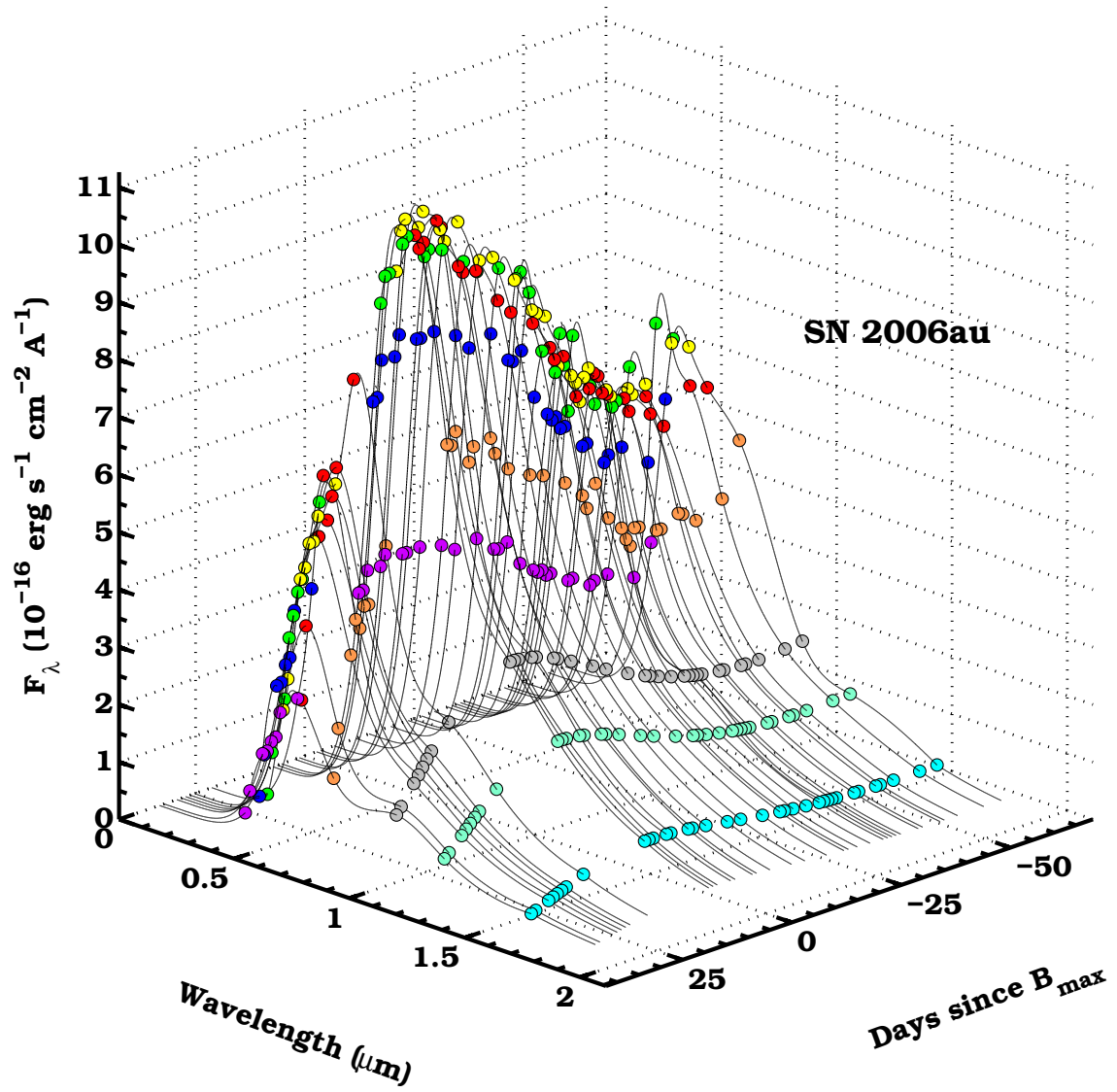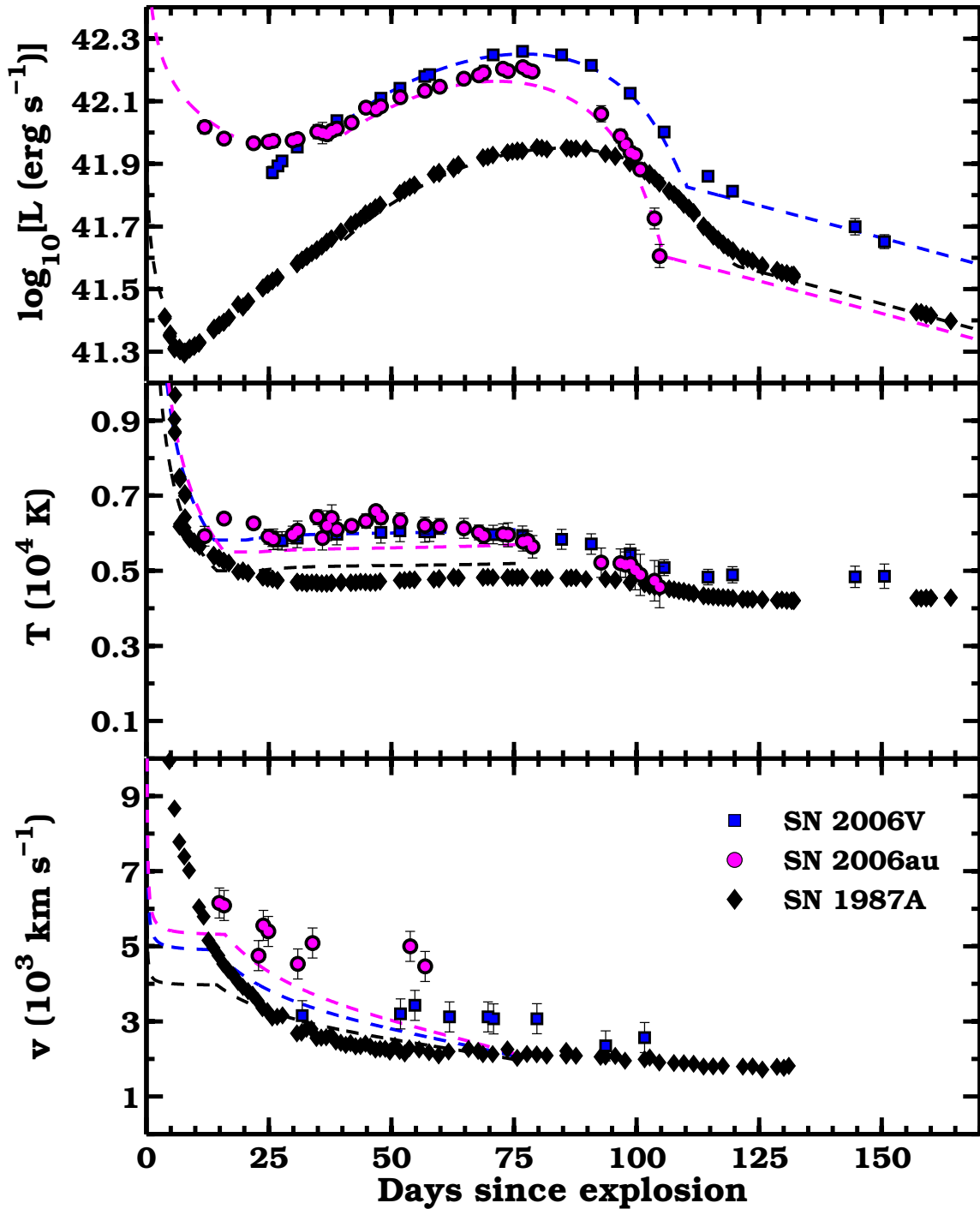
Figure 13: Spectral energy distributions as a function of time for SN 2006au. The colors correspond to those adopted for each band in Fig. 4. The spline fit along with the IR and UV tails are also shown (solid line).

Figure 14: *Top panel:* The bolometric light curves of SNe 2006V, 2006au and 1987A. Filled symbols show the luminosity resulting from the integration of the SEDs. The fit of the semi-analytic model from Imshennik & Popov (1992) is represented with dashed lines. *Middle panel:* Temperature evolution as obtained through black-body fits to the SED for each photometric epoch. *Bottom panel:* Photospheric velocity evolution for SNe 2006V, 2006au and 1987A. For clarity, the errors on temperature and velocity for SN 1987A have been omitted in the plot. These are of the same order as the errors for SNe 2006V and 2006au.
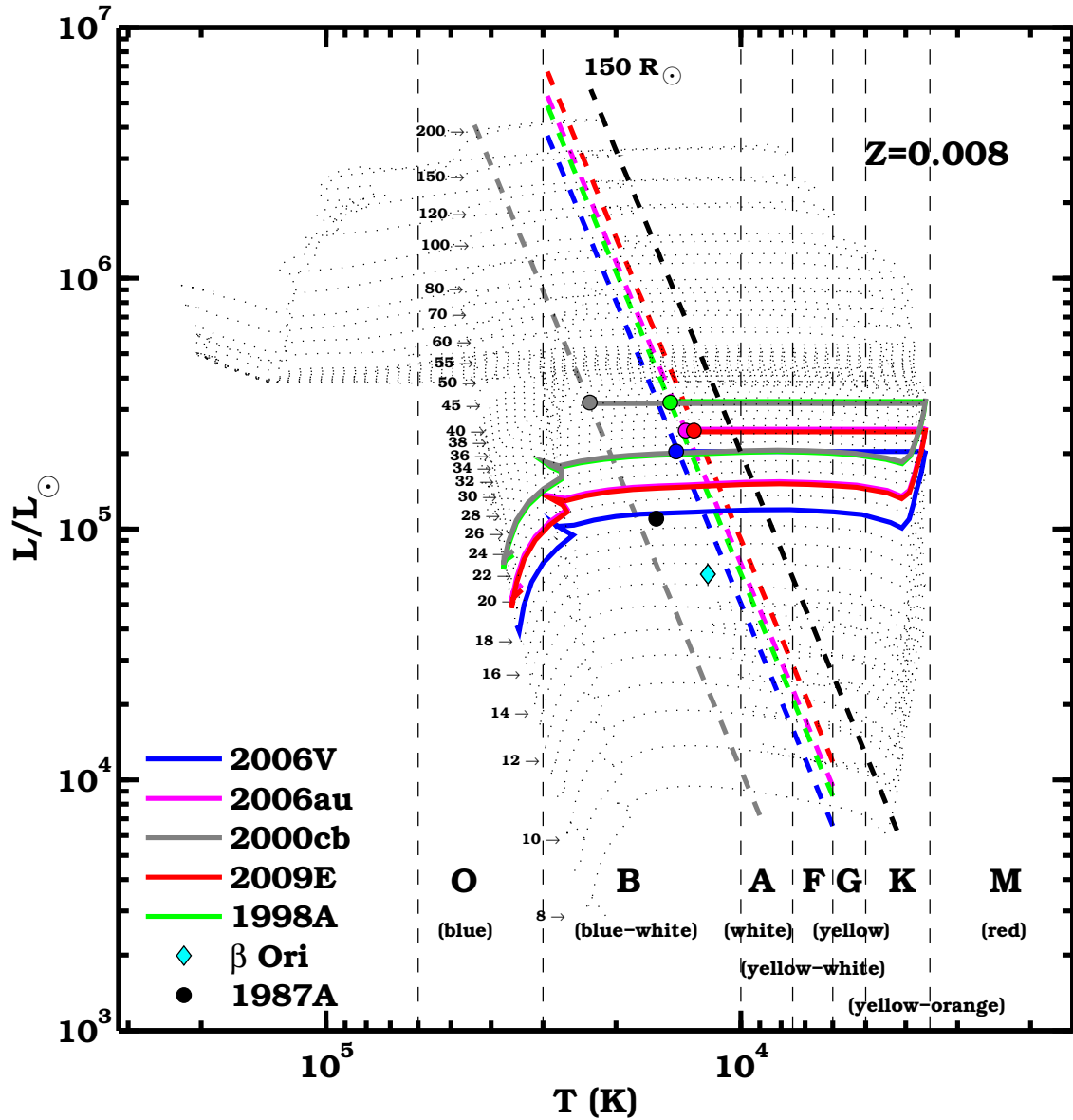
Figure 15: Hertzsprung-Russel diagram for 1987A-like SN progenitors. The evolutionary path for each object (colored solid lines) has been computed with the STARS code (Eldridge & Tout 2004), assuming the progenitor mass from the modeling (ejecta mass plus 2 $M_\odot$ forming the central compact object) and LMC metallicity ($Z = 0.008$, Glatt et al. 2010). The paths for masses ranging between 8 and 200 $M_\odot$ are also shown (dotted lines). The position of each progenitor at the moment of the explosion (colored circles) has been obtained by assuming the progenitor to be a black body emitting with the luminosity of the last epoch of its evolutionary path and having a radius (colored dashed lines) equal to our model estimate. All the 1987A-like SN progenitors belong to the blue-white (B) spectral type as the progenitor of SN 1987A (Woosley 1988). The 150 $R_\odot$ line is shown in the plot for comparison, as well as the position of a well-know BSG, β Orionis (Stewart et al. 2009).